

# Scanning Electron Microscopy

---

Volume 1982  
Number 1 1982

Article 1

---

1982

## Cross Sections for Inelastic Scattering of Electrons by Atoms - Selected Topics Related to Electron Microscopy

Mitio Inokuti  
*Argonne National Laboratory*

Steven T. Manson  
*Georgia State University*

Follow this and additional works at: <https://digitalcommons.usu.edu/electron>

 Part of the [Biology Commons](#)

---

### Recommended Citation

Inokuti, Mitio and Manson, Steven T. (1982) "Cross Sections for Inelastic Scattering of Electrons by Atoms - Selected Topics Related to Electron Microscopy," *Scanning Electron Microscopy*. Vol. 1982 : No. 1 , Article 1.

Available at: <https://digitalcommons.usu.edu/electron/vol1982/iss1/1>

This Article is brought to you for free and open access by the Western Dairy Center at DigitalCommons@USU. It has been accepted for inclusion in Scanning Electron Microscopy by an authorized administrator of DigitalCommons@USU. For more information, please contact [digitalcommons@usu.edu](mailto:digitalcommons@usu.edu).



## CROSS SECTIONS FOR INELASTIC SCATTERING OF ELECTRONS BY ATOMS – SELECTED TOPICS RELATED TO ELECTRON MICROSCOPY\*

Mitio Inokuti

Argonne National Laboratory, Argonne, Illinois 60439

and

Steven T. Manson

Department of Physics and Astronomy  
Georgia State University, Atlanta, Georgia 30303

### ABSTRACT

We begin with a resumé of the Bethe theory, which provides a general framework for discussing the inelastic scattering of fast electrons and leads to powerful criteria for judging the reliability of cross-section data. The central notion of the theory is the generalized oscillator strength as a function of both the energy transfer and the momentum transfer, and is the only non-trivial factor in the inelastic-scattering cross section. Although the Bethe theory was initially conceived for free atoms, its basic ideas apply to solids, with suitable generalizations; in this respect, the notion of the dielectric response function is the most fundamental. Topics selected for discussion include the generalized oscillator strengths for the K-shell and L-shell ionization for all atoms with  $Z \leq 30$ , evaluated by use of the Hartree-Slater potential. As a function of the energy transfer, the generalized oscillator strength most often shows a non-monotonic structure near the K-shell and L-shell thresholds, which has been interpreted as manifestations of electron-wave propagation through atomic fields. For molecules and solids, there are additional structures due to the scattering of ejected electrons by the fields of other atoms.

### 1. INTRODUCTION

Throughout the present article, we consider incident electrons at kinetic energies of interest to microscopy, i.e., between a few tens of keV and several MeV. As targets, we consider first neutral atoms having lower atomic numbers (say,  $Z < 30$ ), and later molecules and solids composed of those atoms. For the majority of the inelastic collisions of electrons with atoms thus delimited, the Bethe theory (Bethe 1930, 1932, 1933) is well justified, and provides a good framework for general understanding and for numerical evaluation of cross sections (Inokuti, 1971; Inokuti et al., 1978).

A necessary (though not sufficient) condition for the first Born approximation, used in the Bethe theory, is that the mean orbital speed of the atomic electron pertinent to the inelastic collision be small compared to the incident electron speed. For ionization (or excitation) of an inner shell by relativistic electrons, the condition means that the effective-charge number  $\zeta$  seen by an atomic electron in that shell be substantially smaller than 137;  $\zeta$  is somewhat smaller than the atomic number  $Z$ , and the condition is fulfilled for moderate  $Z$ , (say  $Z < 30$ ). For the lowest incident energies of electrons we consider, the condition is satisfied only for lower  $Z$ .

The condition discussed above literally applies to *quantitative* discussion of cross sections. Even when the condition is not quite fulfilled, however, often results of the first Born approximation are useful; they may be good as qualitative guides and may be reliable to modest accuracy (perhaps within a factor of two). This is especially the case for inelastic collisions resulting in an optically allowed transition and in small scattering angles; then, the impact parameter is large and thus the incident electron travels well outside the target atom. This recognition is readily verifiable in a variety of empirical data, and is in effect expressible in a more rigorous theoretical form (Lassetre et al., 1969).

Figure 1 exemplifies differential cross sections plotted against the scattering angle  $\theta$ . The figure shows the cross sections for collisions of 25-keV electrons with neon, most of the data being taken from Geiger (1964). Notice that all cross sections are peaked at small angles and that the plot is doubly logarithmic. The elastic-collision cross section is virtually flat at small  $\theta$ , because the interactions between the electron and the atom effectively have a short range in this case. The potential for these interactions decreases with distance  $r$  as  $r^{-4}$

---

\*Work performed under the auspices of the U.S. Department of Energy and of the U.S. Army Research Office.

**Keywords:** Bethe theory, inner shells, generalized oscillator strength, momentum transfer, cross section, inelastic scattering, non-hydrogenic, systematics, Bethe surface, extended x-ray absorption fine structures (EXAFS), hydrogenic approximation.

Contact: Mitio Inokuti, Argonne National Laboratory  
Argonne, Illinois 60439 (312) 972-4186

## LIST OF SYMBOLS

$a_0$	= The Bohr radius, $\hbar^2 / me^2 = 0.52918 \times 10^{-8}$ cm	$\underline{p}'$	= Momentum of an electron after collision
$b$	= Impact parameter	$P_{n\ell}(r)$	= Radial wavefunction for a bound $n\ell$ state
$B$	= Electron binding energy	$P_{\epsilon\ell}(r)$	= Radial wavefunction for a continuum $\epsilon\ell$ state
$c$	= The light speed in vacuum	$Q$	= The recoil energy defined by Eq. (6)
$C_E$	= The constant in Eq. (11)	$r$	= Radial distance
$C_{\text{tot}}$	= The dimensionless constant in Eq. (13)	$\underline{r}_j$	= Position vector of the $j$ -th atomic electron
$C_{\epsilon\ell}$	= The normalization constant for a continuum $\epsilon\ell$ state, Eq. (30)	$R$	= The Rydberg energy, $me^4 / 2\hbar^2 = 13.606$ eV
$d\sigma_E$	= Differential cross section for energy-transfer values between $E$ and $E + dE$	$R(\epsilon, \ell', n, \ell, \lambda, K)$	= The radial integral defined by Eq. (20)
$d\sigma_R$	= The Rutherford cross section	$T$	= Kinetic energy of an incident electron
$df(K, E) / dE$	= The density of the generalized oscillator strength per unit range of energy transfer $E$ , for momentum transfer $\hbar K$	$U$	= The total effective potential defined by Eq. (29)
$dT / dx$	= Stopping power	$v$	= Speed of an electron
$d\omega$	= Solid-angle element	$V(r)$	= The potential of the atomic field of force seen by an electron
$e$	= The charge on an electron	$V_{\text{Hyd}}(r)$	= The potential in the hydrogenic approximation
$E$	= Energy transfer from an incident electron to a target, viz., excitation energy of the target	$V_0$	= The constant in $V_{\text{Hyd}}(r)$ , Eq. (27)
$E_{\text{av}}$	= Mean energy transfer per inelastic collision	$X$	= The variable defined by Eq. (12)
$\hbar$	= The rationalized Planck constant	$Y$	= Electron-exchange term in Eq. (15)
$Im$	= Imaginary part	$Y_{\ell m}(\theta, \phi)$	= Spherical harmonic function
$I_{n\ell}$	= The binding energy of the $n\ell$ subshell	$Z$	= Atomic number
$j_\lambda(Kr)$	= The spherical Bessel function of order $\lambda$ and argument $Kr$	$Z_{\text{eff}}$	= The constant in $V_{\text{Hyd}}(r)$ , Eq. (27)
$\underline{K}$	= Wave vector transferred from an incident electron to a target ( $\hbar\underline{K}$ is momentum transfer)	$Z_i$	= Effective-charge number
$K_{\text{max}}$	= The maximum value of the magnitude of $\underline{K}$	$\beta$	= Speed of an electron measured in the speed of light in vacuum ( $v/c$ )
$K_{\text{min}}$	= The minimum value of the magnitude of $\underline{K}$	$\delta(\quad)$	= Dirac delta function
$k$	= The wave number of an electron	$\epsilon$	= Kinetic energy of an ejected electron
$\ell$	= The orbital angular-momentum quantum number in an initial bound state	$\epsilon_{n\ell}$	= Eigenenergy of the $n\ell$ state
$\ell'$	= The orbital angular-momentum quantum number in a final continuum state	$\epsilon(\underline{K}, E)$	= The complex dielectric response function, which depends on momentum transfer $\hbar\underline{K}$ and energy transfer $E$
$m$	= The magnetic quantum number	$\zeta$	= Effective-charge number (effective atomic number that characterizes an atomic field seen by an inner-shell electron)
$m$	= The electron rest mass	$\eta_E(K)$	= The atomic matrix element defined by Eq. (5)
$M_E^2$	= Dipole matrix element squared for energy transfer $E$ , i.e., a constant in Eq. (11)	$\theta$	= Scattering angle
$M_{\text{tot}}^2$	= Dipole matrix element squared for total inelastic scattering, i.e., a dimensionless constant in Eq. (13)	$\Theta$	= Polar angle
$n$	= Principal quantum number	$\hat{\theta}$	= Aperture angle
$N$	= The number density of atoms	$\sigma_E$	= Cross section for energy-transfer values between $E$ and $E + dE$
$\underline{p}$	= Momentum of an electron before collision	$\sigma_{\text{tot}}$	= Total inelastic-scattering cross section
		$\sigma_{\text{TOT}}$	= The total photoionization cross section of the $K$ shell of molecular nitrogen, shown in Fig. 17
		$\phi$	= Azimuthal angle
		$ 0\rangle$	= The ground state of an atom
		$ E\rangle$	= An excited state of an atom, at excitation energy $E$

## Cross Sections for Inelastic Scattering

or more rapidly. The inelastic-collision cross sections depend on  $\theta$  more strongly and behave as  $\theta^{-2}$  over a moderate range of  $\theta$ , showing that the interactions are of long range (due to the instantaneous dipole moment associated with the atomic transition). The potential for these interactions decreases with distance  $r$  as slowly as  $r^{-2}$ . At larger  $\theta$ , the  $\theta$ -dependence of the inelastic-collision cross section is stronger; the onset of the stronger dependence is different for different atomic shells involved. It is the Bethe theory that enables one to see precisely all these features of the cross sections and to understand how they come about.

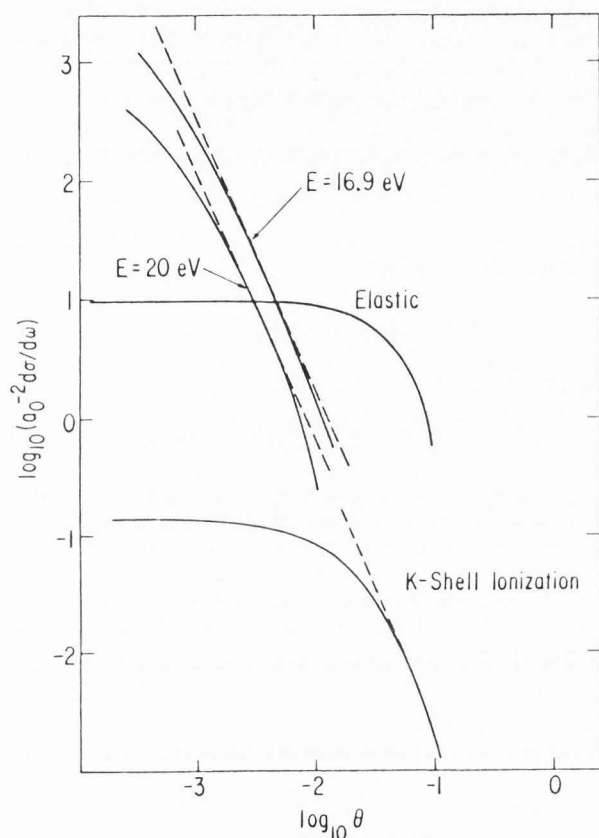


**Fig. 1.** Differential cross sections for collisions of 25-keV electrons with a neon atom.

The horizontal axis represents the common logarithm of the scattering angle  $\theta$ . The vertical axis represents the logarithm of the cross section per unit solid angle  $d\sigma/d\omega$  measured in the squared Bohr radius  $a_0^2 = 0.280 \times 10^{-16} \text{ cm}^2$ . The curve labeled "Elastic" shows the elastic-scattering cross section. The curve labeled "E = 16.9 eV" represents the cross section for the excitation to the  $2p^53s$  state. The curve labeled "E = 20 eV" represents the cross section for the excitation to  $2p^54s$  and all higher states combined. All the above are based on data given by Geiger (1964). The curve labeled "K-Shell Ionization" is based on the theoretical generalized oscillator strength calculated by the present authors. The broken straight lines are drawn to show the  $\theta^{-2}$ -dependence of the cross sections, valid at a range of intermediate  $\theta$  values.

As a prelude to discussion on cross sections, we may note here certain contrasts between the valence shell and the inner shells. The valence shell has a linear dimension of the standard atomic size, i.e., of the order of the Bohr radius  $a_0 = \hbar^2/me^2 = 0.52918 \times 10^{-8} \text{ cm}$ , and has binding energies of the order of the Rydberg energy  $R = me^4/2\hbar^2 = 13.606 \text{ eV}$ . The electronic structure of the valence shell is seriously influenced by subtle effects of many-electron correlations or of the atomic environment (i.e., chemical bonds and condensed-phase formation). Consequently, experimental spectra of the valence shell are rich in general, and often contain keys for unraveling those subtle effects; theoretical calculation of the cross section for valence-shell excitation or ionization is complicated in general and is often difficult in practice. By contrast, an inner shell has a much smaller linear dimension (of the order of  $a_0/\zeta$ ) and a much greater binding energy (of the order of  $\zeta^2 R$ ). Many-electron correlations or atomic-environment effects influence the electronic structure of an inner shell only modestly. Thus, experimental spectra of the inner shell are governed roughly by the atomic number  $Z$ , and therefore often serve as a means of *elemental* chemical analysis. The simple picture of the inner-shell spectra is often taken for granted, but is in fact subject to a provision. The simple picture is right so long as an ejected electron is much more energetic compared to the potential of its interactions with the ion core left behind and with the atomic environment. Otherwise, the ejected electron is slow enough to "see" details of the potential, and gives rise to various observable consequences in the inner-shell spectra. Much of the discussion in Section 3 will concern this topic.

The present article is in effect a continuation of an earlier article (Inokuti, 1978) also written for the electron microscopist. For the reader of that article, the following will serve as an update with an emphasis on newer findings on inner-shell ionization.

## 2. ELEMENTS OF THE BETHE THEORY

### 2.1 Basics

Suppose that an electron of speed  $v$  collides with an atom and excites it to a higher state, either discrete or continuum, at excitation energy  $E$  measured from the ground state. The kinetic energy of the electron then will be reduced by  $E$ , which may be called the energy loss (from the incident electron) or the energy transfer (to the target atom). The direction of the electron motion may be deflected by angle  $\theta$ , which is called the scattering angle.

The *first point* of Bethe is that the momentum transfer  $\hbar\mathbf{K} = \mathbf{p} - \mathbf{p}'$ , where  $\mathbf{p}$  is the momentum before the collision and  $\mathbf{p}'$  is the same after the collision, is the key variable for analyzing any collision of fast particles. The magnitude  $\hbar K$  is readily calculable from  $\theta$ ,  $E$ , and  $v$  by use of elementary kinematics. For electron energies not negligible compared to  $mc^2 = 511 \text{ keV}$ , one must use relativistic kinematics.

The notion of the momentum transfer  $\hbar\mathbf{K}$  may be most easily understandable when one relates it to the notion of the impact parameter  $b$  used in classical mechanics. Indeed, the two notions are complementary in the sense that the relation

$$\hbar K b \cong 1 \quad (1)$$



holds for the majority of collisions. In other words, collisions at large  $b$  are called soft or glancing, and result in small  $K$ ; collisions at small  $b$  are called hard or knock-on, and result in large  $K$ . Nevertheless, there is a fundamental distinction; the momentum transfer is unambiguously defined in all cases, while the impact parameter is not a quantum-mechanical observable. [See Section 4.4 of Inokuti 1971 and Bohr 1948.]

For fixed  $v$  and  $E$ , the momentum transfer  $\hbar K$  may take a range of values depending on  $\theta$ . The smallest value of  $\hbar K$  occurs when  $\theta = 0$ , and is given by

$$\hbar K_{\min} \equiv E/v. \quad (2)$$

To derive this, one relates the change  $\Delta p$  in the electron momentum  $p$  with the change  $\Delta T$  in the kinetic energy  $T$  as  $\Delta p = (dp/dT)\Delta T$ , sets  $\Delta p = \hbar K_{\min}$  and  $\Delta T = E$ , and notes  $dT/dp = v$ . The derivation, as well as the result [Eq. (2)], is correct in both relativistic and non-relativistic kinematics. Notice that  $\hbar K_{\min}$  for any inelastic collision is never vanishing, although it becomes smaller and smaller with increasing  $v$  or with decreasing  $E$ . The largest value of  $\hbar K$  for fixed  $v$  occurs when  $\theta = \pi$ , and is about twice the incident momentum, i.e.,

$$\hbar K_{\max} \equiv 2mv/(1-\beta^2)^{1/2}, \quad (3)$$

where  $\beta = v/c$  and  $m$  is the electron rest mass. Thus,  $\hbar K_{\max}$  is in general large and increases without bounds as  $v \rightarrow c$ .

The *second point* of Bethe concerns the differential cross section for energy transfer values between  $E$  and  $E + dE$

$$d\sigma_E = 4a_0^2(p'/p)(Ka_0)^{-4} |\eta_E(K)|^2 2\pi \sin\theta d\theta, \quad (4)$$

where  $\eta_E(K)$  is an atomic matrix element

$$\eta_E(K) = (E | \sum_{j=1}^Z \exp(i\mathbf{K} \cdot \mathbf{r}_j) | 0) \quad (5)$$

taken between the excited state  $(E |$  and the ground state  $|0)$ ,  $\mathbf{r}_j$  being the position of the  $j$ th atomic electron. The quantity  $|\eta_E(K)|^2$  is called a form factor for inelastic scattering, and may be taken as an even function of scalar  $K$ , so long as the target atoms or molecules are randomly oriented. Equations (4) and (5), as well as several equations to follow, are written specifically for non-relativistic speeds  $v$ , for the sake of compact expression. Notice that  $d\sigma_E$  has the dimension area<sup>2</sup> energy<sup>-1</sup> and  $|\eta_E(K)|^2$  has the dimension energy<sup>-1</sup>.

We may rewrite Eq. (4) to express  $d\sigma_E$  in terms of the momentum transfer  $\hbar K$  or other related variables. For instance, one may introduce a variable with the energy dimension, i.e.,

$$Q = (\hbar K)^2/2m \quad (6)$$

and write

$$d\sigma_E = (2\pi e^4/mv^2) |\eta_E(K)|^2 Q^{-2} dQ. \quad (7)$$

Here it is appropriate to recall the Rutherford formula, which applies to collisions of two free charged particles. Specifically for a collision of an electron with a free and stationary electron, the Rutherford cross section reads

$$d\sigma_R = (2\pi e^4/mv^2) Q^{-2} dQ, \quad (8)$$

and  $Q$  represents in this hypothetical instance the kinetic energy of the recoiled electron. Thus the meaning of the form factor  $|\eta_E(K)|^2$  becomes clear; it represents the ratio of the atomic cross section  $d\sigma_E$  to the Rutherford cross section. It is the only nontrivial factor in  $d\sigma_E$  in the sense that its evaluation by means of Eq. (5) presumes knowledge of atomic structure. To summarize, we owe to Bethe (then twenty-four years old) the crucial recognition that  $d\sigma_E$  factorizes into the Rutherford cross section (which depends on the incident-particle variables only) and the form factor (which depends on target properties but not explicitly on the incident speed  $v$  or any other incident particle variable). For more detailed commentary, see Inokuti (1971) and Inokuti (1978).

Finally, the generalized oscillator strength  $df(K,E)/dE$  per unit range of  $E$  is defined by

$$df(K,E)/dE = (E/Q) |\eta_E(K)|^2. \quad (9)$$

Equivalently, we may write

$$df(K,E)/dE = (E/R)(Ka_0)^{-2} |\eta_E(K)|^2. \quad (10)$$

The equivalence of Eq. (10) with Eq. (9) is apparent as soon as one recalls that  $Ra_0^2 = (me^4/2\hbar^2)(\hbar^2/me^2)^2 = \hbar^2/2m$ . The term "generalized oscillator strength" is another innovation of Bethe. As  $K \rightarrow 0$ , it reduces to the optical (dipole) oscillator strength, which governs the light absorption and practically all optical properties of the atom under consideration. For the basics of photoabsorption by atoms, see Fano and Cooper (1968), Manson (1976), Manson (1977), Manson (1978), Manson and Dill (1978), and Starace (1982).

## 2.2 The Bethe Surface

The main object of study is the form factor  $|\eta_E(K)|^2$  or the generalized oscillator-strength density  $df(K,E)/dE$  as a function of both  $\hbar K$  and  $E$ . To make this point clear, Inokuti (1971) used the term "Bethe surface."

We have already discussed the connection with the photoabsorption, which corresponds to the limit ( $K \rightarrow 0$ ) we mentioned at the end of the last Subsection 2.1.

At larger  $E$  values,  $df(K,E)/dE$  substantially differs from zero only when  $Q$  of Eq. (6) nearly equals  $E$  and far exceeds an atomic-shell binding energy. Then,  $df(K,E)/dE$  shows a marked peak at those values of  $K$  and  $E$  which correspond to free-electron collision thus satisfying the relation  $Q = E$ . Inokuti (1971) called the peak *the Bethe ridge*, and emphasized its universal occurrence.

Figure 2 shows the Bethe surface for atomic hydrogen (Inokuti 1971). Figure 3 shows two examples that have been determined by experiment (Lahman-Bennani et al., 1979, 1980).

## Cross Sections for Inelastic Scattering

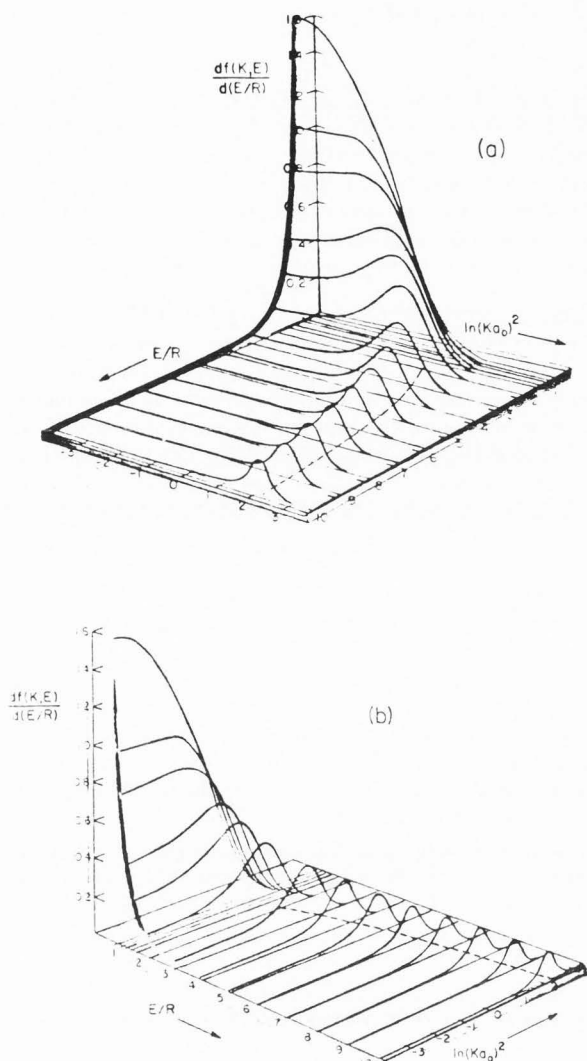


**Fig. 2.** The Bethe surface for atomic hydrogen.

The horizontal axes for  $E/R$  and  $\ln(Ka_0)^2$  define the base plane. The vertical axis represents  $df(K,E)/d(E/R)$ . The fourteen plates are placed  $E/R = 3/4, 8/9, 1, 5/4, 3/2, 2, 3, 4, 5, 6, 7, 8, 9,$  and  $10$ . The broken curve on the base plane shows the location  $(E/R) = (Ka_0)^2$  of the Bethe ridge, which is the main feature for  $E/R \gg 1$ ; collisions represented by a point near the Bethe ridge occur as though the incident particle were to strike a free electron, the electron binding being of secondary importance. The optical region  $(Ka_0)^2 \ll 1$  is conspicuous only for small  $E/R$ . Figure 2a shows the gradual spreading of the Bethe ridge with decreasing  $E/R$ , and eventually its merger with the optical plateau at the region of small  $(Ka_0)^2$  and  $E/R$ . Figure 2b shows in front a cut at  $\ln[(Ka_0)^2] = -4$ , i.e., a curve that closely approximates the photoabsorption cross section. This figure is taken from Inokuti (1971).

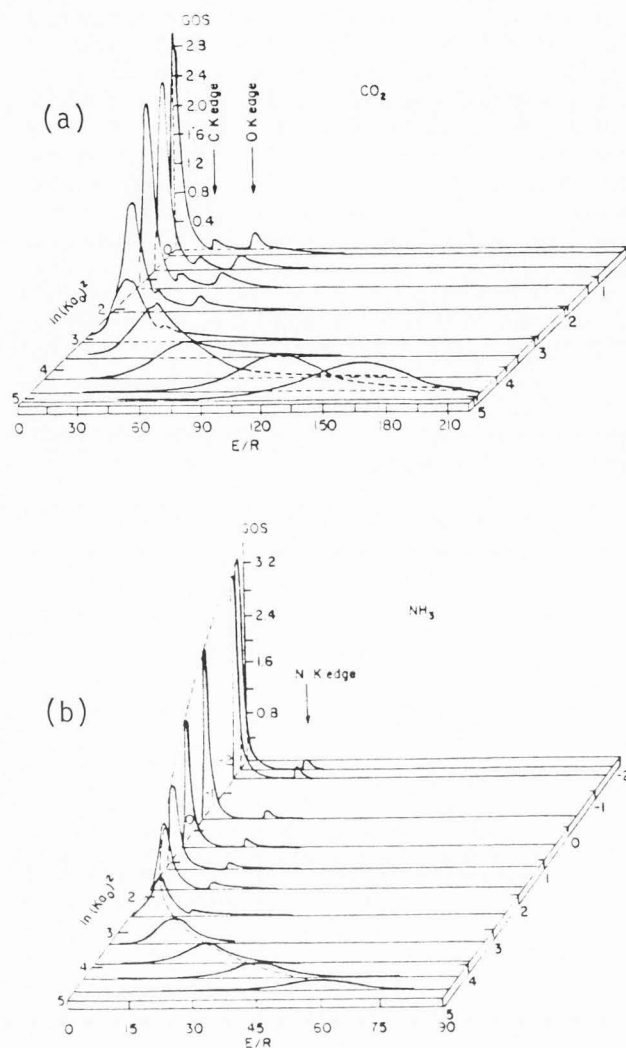


**Fig. 3.** The Bethe surfaces of carbon dioxide (Fig. 3a) and ammonia (Fig. 3b), after Lahmam-Bennani et al. (1979), 1980), reproduced with permission by the authors and the publishers.

The base plane is defined by  $E/R$  (the energy transfer measured in the Rydberg energy, 13.6 eV) and by  $\ln[(Ka_0)^2]$  (in the notation of the present article). The dashed curve indicates the Bethe ridge for valence electrons. Notice the K-shell ionization contributions near the threshold energies of carbon, nitrogen, and oxygen atoms.

The study of the Bethe surface is a rich subject with many applications and implications to diverse phenomena. Just to name several examples, we may start with sum rules, which usually mean theorems on the integrals involving  $df(K,E)/dE$  with respect to  $E$  (including sums over discrete spectra), at fixed  $K$ . These sum rules (Section 3.3 of Inokuti 1971) are often useful as control on data. There are also theorems on the integrals involving  $df(K,E)/dE$  with respect to  $K$ , at fixed

E. (See Section IIE of Inokuti et al., 1978, and Matsuzawa et al., 1979). If the Bethe surface is drawn on the plane with Cartesian axes representing  $E$  and  $\ln K$ , then the volume under the surface delimited by appropriate kinematic limits represents the stopping power of the target atom for any fast charged particle (Bethe 1930, and Section 4.3 of Inokuti 1971). The shape of the Bethe ridge is a reflection of electron binding in atoms, or more precisely, the electron momentum distribution, and is connected with the Compton profile, i.e., the spectral distribution of high-energy photons scattered by atomic electrons (Bonham and Wellenstein 1973, Wong et al., 1975, Barlas et al., 1977, and Lahman-Bennani et al. (1979, 1980)). Finally, the so-called (e,2e) measurements, i.e., coincidence measurements of scattered electrons and ejected electrons resulting from collisions corresponding to the Bethe ridge, represent an area of many recent studies (McCarthy and Weigold 1976).

### 2.3 Integrated Cross Sections and Their Systematics

The *third point* of Bethe concerns the cross section integrated over all scattering angles. Starting with Eqs. (4)-(7) and using general properties of the form factor or of the generalized oscillator strength, one can show that

$$\sigma_E = 8\pi a_0^2 (R/mv^2) (M_E^2 X + C_E), \quad (11)$$

where

$$X = \ln[\beta^2/(1 - \beta^2)] - \beta^2, \quad (12)$$

and  $M_E^2$  and  $C_E$  are atomic properties derivable from  $df(K,E)/dE$ . What is most important here is that the dependence of  $\sigma_E$  on the electron speed  $v = \beta c$  is analytically given and is universal for all targets.

As a consequence, the total inelastic-collision cross section  $\sigma_{tot}$ , i.e., the sum of all inelastic-collision cross sections, is given by a formula of the same general structure, i.e.,

$$\sigma_{tot} = 8\pi a_0^2 (R/mv^2) (M_{tot}^2 X + C_{tot}), \quad (13)$$

where  $M_{tot}^2$  and  $C_{tot}$  are atomic properties that often allow accurate evaluation. (See Section 4.3 of Inokuti 1971 and Inokuti et al., 1967). An application of this result is now demonstrated in Fig. 4 and Fig. 5 (adapted from Inokuti et al., 1981). Figure 4 shows  $\sigma_{tot}$  for 50-keV electron for all atoms with  $Z \leq 38$ . Notice the periodic variation with  $Z$ , due to the well-known structure of atoms.

Another consequence of Eq. (11) is the famous Bethe formula for the stopping power  $dT/dx$ , i.e., the mean energy loss per unit path length of a charged particle penetrating through a medium. It may be evaluated as

$$dT/dx = N \int E \sigma_E dE \quad (14)$$

for a medium having the number density of atoms  $N$ , where the integration runs over the whole range of energetically possible  $E$  values belonging to continuous and discrete spectra. The integral is called the stopping cross section  $\sigma_{st}$ , and has the dimension area<sup>2</sup> energy. The Bethe formula for an electron may be written as

$$\sigma_{st} \approx 16\pi a_0^2 (R^2/mv^2) Z [X + \ln(2mc^2/I) + Y], \quad (15)$$

where  $X$  is the variable defined by Eq. (12). The term  $Y$  represents electron-exchange effects; it is a function of  $\beta$  and amounts to about ten percent of the other terms in the square brackets. For precise treatment, see Bethe (1932, 1933) and Section 4.3 of Inokuti (1971). More importantly, Eq. (15) contains a single nontrivial property of the medium atom, i.e., the mean excitation energy  $I$ , which is defined in terms of the dipole oscillator-strength density as

$$\ln I = \int \ln E [df(0,E)/dE] dE / \int [df(0,E)/dE] dE \quad (16)$$

The integral in the denominator is equal to the atomic number  $Z$  according to the well-known sum rule. The mean excitation energies for various materials are an object of extensive studies, as seen in Inokuti and Turner (1978) and in Inokuti et al. (1981). The ratio  $I/Z$  is a function of  $Z$ , exhibits minima and maxima reflecting the atomic shell structure for lower  $Z$ , and tends to a limiting value of about 10 eV for high  $Z$ .

As an application of Eqs. (13) and (15), one may consider the mean energy transfer per inelastic collision, viz.,

$$E_{av} = \sigma_{st} / \sigma_{tot}. \quad (17)$$

This quantity is of great interest to the electron microscopist for consideration of the radiation damage of specimens and other related matters. Figure 5 shows the mean energy transfer  $E_{av}$  per inelastic collision, for 50-keV electrons (chained dash) and for protons at the same speed (solid line), as functions of  $Z$ . As Inokuti (1978) pointed out, electron microscopists often use theoretical values of  $\sigma_{tot}$  and  $E_{av}$  based on the Thomas-Fermi model of atoms. This model treats all atomic electrons as a free-electron gas, disregards the atomic shell structure, and therefore naturally predicts  $\sigma_{tot}$  and  $E_{av}$  as smooth functions of  $Z$ .

### 2.4 Condensed Phases

Bethe treated free atoms as target. Extension to free molecules is formally straightforward. In the definition of the matrix element  $\eta_E(K)$  [Eq. (5)] molecular eigenfunctions must be used, and the rotational and vibrational degrees of freedom must be accounted for. Despite the complications, the theory remains basically unchanged. For fuller discussion, Section 3.5 of Inokuti (1971).

Extension to condensed phases began with the work of Fermi (1940), who pointed out what we call the density effect on energy losses. For a relativistic particle traveling through condensed matter, the relevant impact parameter may become so large that there are many medium atoms between the particle and a particular atom that becomes excited. To see this, recall Eqs. (1) and (2); the maximum impact of parameter is  $1/K_{min} \cong \hbar c/E$ , and becomes  $2 \times 137 a_0 = 145 \text{ \AA}$  for  $E = R$ . The medium atoms are instantaneously polarized by the electric field of the particle and tend to screen the particle interactions with the atom that eventually receives energy. Fermi used a macroscopic description according to electrodynamics, as summarized by Landau and Lifshitz (1960).

### Cross Sections for Inelastic Scattering

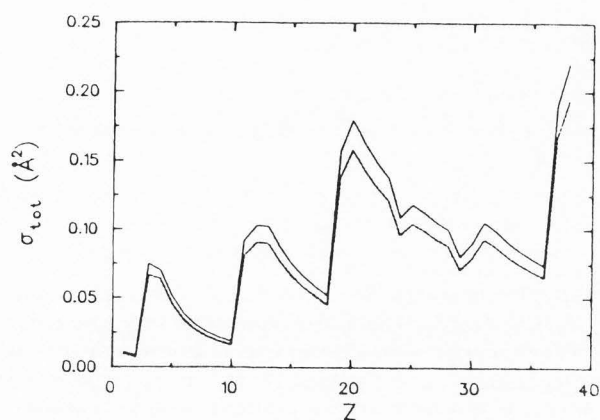


**Fig. 4.** The total inelastic-scattering cross section  $\sigma_{\text{tot}}$  (measured in  $\text{\AA}^2$ ) for 50-keV electrons, plotted against atomic number  $Z$ .

The solid line shows the result of calculations that incorporate relativistic kinematics for the incident electron. For comparison, the dotted line shows the results of calculations that disregard relativistic kinematics. The figure is taken from Inokuti et al. (1981).

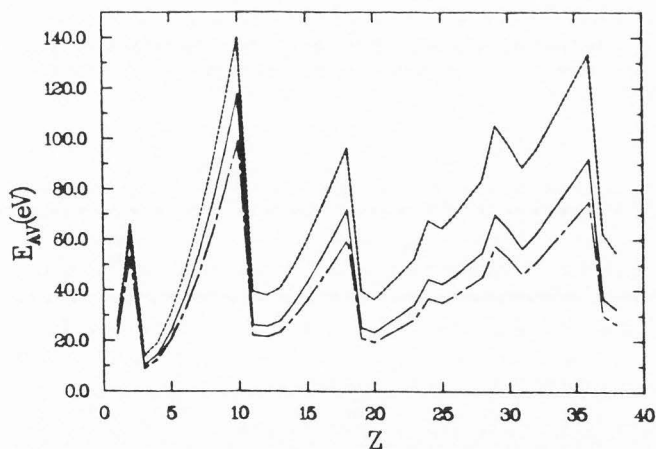


**Fig. 5.** The mean energy transfer  $E_{\text{AV}}$  per inelastic collision (measured in eV), plotted against atomic number  $Z$ .

The general features of the curve  $Z$ -dependence are the same for all charged particles incident with sufficiently high speed. The solid line is for a proton at 91.8 MeV (viz.,  $\beta = 0.4127$ ). The chained dash line is for an electron at 50-keV (viz., the same  $\beta$ ). The stopping power for an electron is smaller than that for a proton of the same speed when one accounts for the exchange of the primary electron with a secondary electron in close collisions. The dotted line shows a limiting  $E_{\text{AV}}$  for any extremely relativistic charged particle. The figure is based on the data given by Inokuti et al. (1981).

More detailed treatments were developed in the 1950's by many workers including Fano (1956), Ferrell (1957), and Nozières and Pines (1959). Special attention was paid to plasmon excitations in metals, which then began to be studied through electron energy-loss measurements. Recent work on plasmon excitation is reviewed by Raether (1980). The following paper by Powell (1983) in the present Conference describes general features of electron inelastic scattering in solids and relevant cross sections.

Here we make only a few remarks. The three major points of Bethe (i.e., the role of the momentum transfer, the factorization of the cross section into the Rutherford factor and the form factor, and the analytic structure of the integrated cross section) all remain true for condensed phases. The form-factor idea is generalized, and it is customary to use the complex dielectric response function  $\epsilon(\underline{K}, E)$  for describing the effects of electromagnetic perturbation associated with angular frequency  $E/\hbar$  and propagation vector  $\underline{K}$ . The function may be interpreted also as the Fourier transform of the electron density fluctuation in the medium. For charged-particle interactions, the quantity  $E \text{Im}[-1/\epsilon(\underline{K}, E)]$  plays the role of the generalized oscillator strength  $df(\underline{K}, E)/dE$ .

The use of the complex function  $\epsilon(\underline{K}, E)$  entails studies on the analytic properties, especially on the integral relations between the real and imaginary parts, called Kramers-Kronig dispersion relations. Thorough exploitation of these relations has been carried out for several instances, e.g., metallic aluminum (Shiles et al., 1980), but *only* for data at  $\underline{K} = 0$ .

### 3. SELECTED TOPICS

#### 3.1 Generalized Oscillator Strengths for Inner Shells of Atoms: Methods of Calculations

Earlier calculations on the generalized oscillator strengths of inner shells and related quantities were based on the hydrogenic approximation (Walske 1952, Walske 1956, and Khandelwal and Merzbacher 1966, to name just three examples). In this scheme, one uses for one-electron eigenfunctions for both the initial state and the final state hydrogenic functions, but accounts for the screening by other electrons by means of a suitable effective nuclear charge by an adjustment of the energy scale to fit the experimental ionization threshold. Then, the generalized oscillator strengths may be readily evaluated analytically. Yet, the procedure is intrinsically unrealistic for values of the energy transfer  $E$  comparable with the ionization threshold; this deficiency is serious because much of the strength lies precisely at those  $E$  values for small and moderate  $\underline{K}$  values.

Manson (1972a, 1972b) initiated more realistic calculations, within the one-electron orbital picture. In this picture, one approximates the ground state  $|0\rangle$  of the whole atom by a suitably antisymmetrized product of one-electron orbitals of the form  $r^{-1}P_{nl}(r) Y_{lm}(\Theta, \phi)$ , where  $(r, \Theta, \phi)$  are the spherical coordinates of an atomic electron,  $P_{nl}(r)$  is the radial function with the principal quantum number  $n$  and the orbital angular-momentum quantum number  $l$ ,  $Y_{lm}(\Theta, \phi)$  is the spherical harmonic, and  $m$  is the magnetic quantum number. At the same time, one approximates the excited state  $|E\rangle$  in the continuum by  $r^{-1}P_{\ell' m'}(r) Y_{\ell' m'}(\Theta, \phi)$ , where  $P_{\ell' m'}(r)$  is



the radial function representing an electron ejected with kinetic energy  $\epsilon$  and angular momentum  $\ell'$ . For the ionization of the  $n\ell$  shell having the binding energy  $I_{n\ell}$ ,  $\epsilon$  is related to the energy transfer  $E$  by

$$E = \epsilon + I_{n\ell}. \quad (18)$$

For the transition of an electron from the  $n\ell$  subshell to the ionized state, one may write the atomic matrix element squared as

$$|\eta_E(K)|^2 = (2\ell' + 1)\Sigma_\lambda(2\lambda + 1) \left| \begin{pmatrix} \ell' & \lambda & \ell \\ 0 & 0 & 0 \end{pmatrix} \right|^2 [R(\epsilon, \ell', n, \ell, \lambda, K)]^2, \quad (19)$$

where  $\begin{pmatrix} \ell' & \lambda & \ell \\ 0 & 0 & 0 \end{pmatrix}$  is the Wigner 3j symbol, the sum over the index  $\lambda$  runs from  $-|\ell - \ell'|$  to  $\ell + \ell'$  in steps of 2, and  $R(\epsilon, \ell', n, \ell, \lambda, K)$  is the radial matrix element defined by

$$R(\epsilon, \ell', n, \ell, \lambda, K) = \int_0^\infty P_{\ell'}(r) j_\lambda(Kr) P_{n\ell}(r) dr, \quad (20)$$

$j_\lambda(Kr)$  being the spherical Bessel function of the  $\lambda$ th order. In Eq. (19), the radial matrix element is the only quantity that depends on the dynamics of atomic electron, all the other factors being geometric, i.e., dependent only upon angular-momentum quantum numbers.

The most crucial part of the calculation is the determination of the radial functions  $P$ 's. The function  $P_{n\ell}(r)$  for a bound state with a discrete eigenenergy  $\epsilon_{n\ell} < 0$  satisfies the radial Schrödinger equation

$$\frac{\hbar^2}{2m} \frac{d^2 P_{n\ell}}{dr^2} + \left[ \epsilon_{n\ell} - V(r) - \frac{\hbar^2 \ell(\ell + 1)}{2mr^2} \right] P_{n\ell} = 0, \quad (21)$$

behaves as  $r^{\ell+1}$  for small  $r$ , and vanishes rapidly for large  $r$  so that it may be normalized as

$$\int_0^\infty [P_{n\ell}(r)]^2 dr = 1. \quad (22)$$

In Eq. (21),  $V(r)$  is the potential of the field of force seen by the electron, and the field is due to all the other atomic electrons and the nucleus. For a neutral atom of atomic number  $Z$ , the general limiting behavior is

$$V(r) \cong -Ze^2/r \quad \text{for } r \cong 0, \quad (23)$$

and

$$V(r) \cong -e^2/r \quad \text{for } r \rightarrow \infty. \quad (24)$$

In many calculations including Manson's (1972a, 1972b),  $V(r)$  is determined through a version of self-consistent field theories, called the Hartree-Slater method.

The function  $P_{\ell'}(r)$  for a final, continuum state with energy  $\epsilon > 0$  satisfies the same equation

$$\frac{\hbar^2}{2m} \frac{d^2 P_{\ell'}}{dr^2} + \left[ \epsilon - V(r) - \frac{\hbar^2 \ell(\ell + 1)}{2mr^2} \right] P_{\ell'} = 0, \quad (25)$$

behaves as  $r^{\ell+1}$  for small  $r$ , and is to be normalized as

$$\int_0^\infty P_{\ell'}(r) P_{\ell''}(r) dr = \delta(\epsilon - \epsilon'). \quad (26)$$

Notice that the same potential  $V(r)$  is used in Eq. (25) as in Eq. (21); the use of the same  $V(r)$  not only simplifies the calculation, but also guarantees its internal self-consistency.

The contrast of the modern calculation with the hydrogenic approximation is seen in the choice of the potential  $V(r)$ . The hydrogenic approximation amounts to using

$$V_{\text{Hyd}}(r) = -Z_{\text{eff}} e^2/r + V_0, \quad (27)$$

where  $Z_{\text{eff}}$  and  $V_0$  are two adjustable parameters. This potential  $V_{\text{Hyd}}(r)$  satisfies neither of the two limiting forms, Eqs. (23) and (24). Therefore, the hydrogenic approximation gives no realistic behavior of radial wavefunctions for  $r \cong 0$  or for  $r \rightarrow \infty$ , nor trustworthy results for properties depending upon the behavior of the wavefunctions at large or small  $r$ . An example of such properties is the generalized oscillator strength near a threshold energy ( $\epsilon = 0$ ), which crucially depends upon the radial wavefunctions at larger  $r$ , as we shall fully document in Subsection 3.2.

Many properties of the realistic potential  $V(r)$  have been extensively studied (Rau and Fano 1968); their consequences to radial wavefunctions  $P$ 's have been elucidated in great detail (Fano et al. 1976, Manson 1976, Manson 1977, Manson 1978, Manson and Dill 1978), especially in connection with the optical oscillator strength spectra, i.e.,  $df(K, E)/dE$  at the limit  $K \rightarrow 0$ . Calculations by Manson (1972a, 1972b) and their extensions (Manson and Inokuti, 1980) are based on extensive experience with work on the optical oscillator strength. Manson and Inokuti (1980) have calculated the spectra of the generalized oscillator strengths for the ionization of the K-shell and the L-shell of all atoms for  $Z \leq 30$ , but have not published the results comprehensively. In the following section (Section 3.2), some of the results will be discussed.

Leapman et al. (1980) and Rez and Leapman (1981) also reported similar calculations on the K-, L-, and M-shell generalized oscillator strengths and related quantities for a selection of atoms, based on virtually the same method as that of Manson and Inokuti (1980). McGuire (1977, 1979) carried out similar work as well. But his method contains an additional mathematical approximation; he divides the full  $r$ -range ( $0 < r < \infty$ ) into several intervals, in each of which the potential  $V(r)$  is approximated by a Coulomb potential  $-Z_i e^2/r$  with a suitable effective charge number  $Z_i$ . This allows one to write down the solution in that interval as a linear combination of regular and irregular Coulomb functions and then to determine the coefficients of the linear combination by requirement of smooth connection of the radial wavefunctions. This procedure may very well be more efficient than the straightforward numerical solution of Eqs. (17) and (21), done by Leapman et al. (1980) and by Manson



### Cross Sections for Inelastic Scattering

and Inokuti (1980), but has a definite possibility of generating spurious results.

Finally, calculations more accurate than the Hartree-Slater potential field method are indeed possible, for example, by the use of the Hartree-Fock method, the random-phase approximation, or the method of configuration mixing. Yet, as far as the properties of a deep inner-shell are concerned, more accurate calculations are unlikely to alter drastically the results of the Hartree-Slater calculations. The reason for this expectation comes from the well-known notion of the perturbation theory; the possible corrections to the Hartree-Slater calculations must arise from the perturbative contributions from virtual excited states, but these states are located at very high excitation energies when one deals with a deep inner-shell state.

### 3.2 Generalized Oscillator Strengths for Inner Shells of Atoms: Results

The most suitable way to show the data of the generalized oscillator strength is the plot first given by Miller and Platzman (1957). By use of Eqs. (4), (7), (9), and (10), one can readily see that it is suitable to plot  $df(K,E)/dE$  at fixed  $E$  as a function of  $\ln[(Ka_0)^2]$ . Equivalently, one may plot  $Q^{-1}|\eta_E(K)|^2$  as a function of  $\ln Q$ . Then, the area under the curve represents the integrated cross section over a range of the momentum transfer  $\hbar K$  (or over a range of the scattering angle). To show this point precisely, we may rewrite Eq. (7) as

$$d\sigma_E = \frac{8\pi a_0^2 R}{mv^2} \frac{R}{E} \frac{df(K,E)}{dE} d[\ln(Ka_0)^2]. \quad (28)$$

For fixed incident electron speed  $v$  and fixed energy loss  $E$ , the momentum transfer is uniquely calculable through kinematics. Therefore, the Miller-Platzman plot is a graphical representation of the angular distribution of inelastically scattered electrons at fixed  $v$  and  $E$ . Yet, it takes some time and experience for anyone to become fully familiar with the relation between  $\theta$  and  $(Ka_0)^2$ . As an aid to this end, we present here Fig. 6, which shows the relation for energy-transfer values corresponding to the K-shell threshold ( $E = 1.57$  keV) and to the 2s-subshell threshold ( $E = 127$  eV) of aluminum. The figure illustrates several points. First,  $(Ka_0)^2$  varies over a wide range with varying  $\theta$ . Second, the range of the variation in  $(Ka_0)^2$  becomes greater and greater with increasing incident speed  $v$ . Third,  $(Ka_0)^2$  depends weakly on  $\theta$  for sufficiently small  $\theta$ , but becomes roughly proportional to  $\theta^2$  at large  $\theta$ ; the transition between the two kinds of dependence occurs at smaller and smaller  $\theta$  with increasing  $v$ .

Several of the following figures are examples of the Miller-Platzman plot showing the results of calculations by Manson and Inokuti (1980) for selected atoms. These figures also show the corresponding results of the hydrogenic approximation. Manson and Inokuti have actually calculated and plotted the generalized oscillator-strength density  $df(K,E)/dE$  ( $E/R$ ) for the ionization from the 1s, 2s, and 2p orbits of all atoms through Zn ( $Z = 30$ ). We shall respond to any reasonable request for providing any of the numerical or graphical data we have at hand.

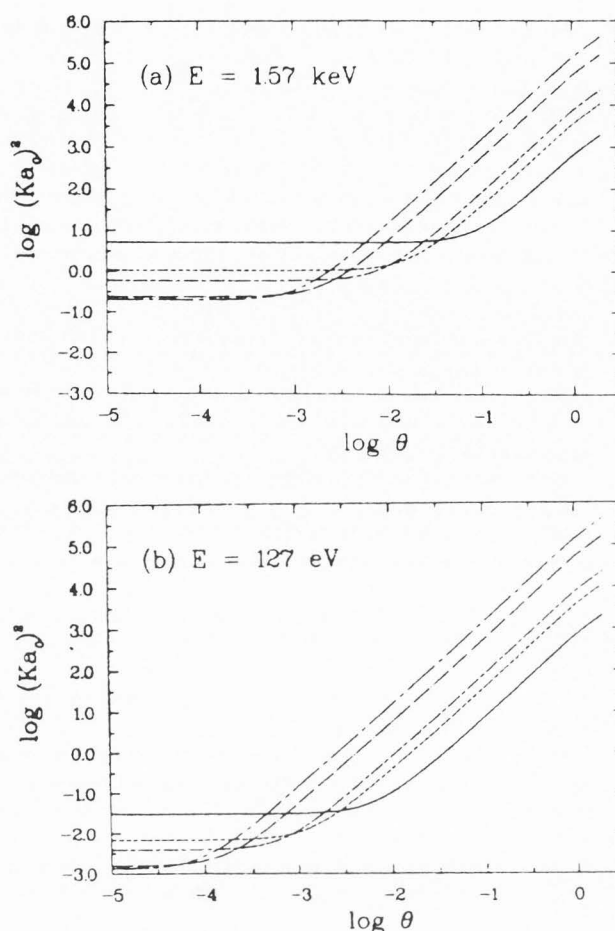


Fig. 6. The relation between  $\theta$  and  $(Ka_0)^2$ .

Suppose that the incident electron has kinetic energy  $T$  and momentum  $p$ , then  $T + mc^2 = [(cp)^2 + (mc^2)^2]^{1/2}$ . Suppose that the scattered electron has kinetic energy  $T'$  and momentum  $p'$ , then  $T' + mc^2 \equiv [(cp')^2 + (mc^2)^2]^{1/2}$ . The energy loss  $E$  is defined by  $T' = T - E$ . The squared momentum transfer is given by  $(\hbar K)^2 = p^2 + p'^2 - 2pp' \cos\theta$ . These relations enable one to calculate  $(Ka_0)^2$  for a given set of  $T$ ,  $E$ , and  $\theta$ . Here we show  $\log_{10}(Ka_0)^2$  as a function of  $\log_{10}\theta$ , for fixed  $T$  and  $E$ . Figure 6a shows the relation for  $E = 1.57$  keV, corresponding to the threshold for K-shell ionization of aluminum. Figure 6b shows the same relation for  $E = 127$  eV, corresponding to the threshold for the 2s-subshell ionization of aluminum. In each case, five curves refer to different kinetic energies  $T$  of the incident electron: 10 keV (—), 50 keV (---), 100 keV (- · - ·), 500 keV (— · — ·), and 1 MeV (— · — ·). For the lowest  $T$  (10 keV), the curve for each  $E$  starts highest at small  $\theta$  and ends lowest at large  $\theta$ . For higher and higher  $T$ , the curve covers wider and wider ranges. Comparison of Fig. 6a and Fig. 6b readily indicates that, for fixed  $T$  and for the same  $\theta$  interval, the range of  $(Ka_0)^2$  values is wider for smaller  $E$  (i.e., in Fig. 6b).

Figures 7-11 concern aluminum. Let us discuss each of them in turn. Figure 7 shows results for the ionization of the 2s-subshell, which has the binding energy  $B = 127$  eV according to Shirley et al. (1977). Each curve represents the density  $df(K,E)/d(E/R)$  of the generalized oscillator strength per unit range of  $E/R = (\epsilon + B)/R$ , where  $\epsilon$  is the kinetic energy of an ejected electron. Figure 7a shows results for the lowest  $\epsilon$  values, i.e.,  $\epsilon/R = 0, 0.5, 1.0, 1.5,$  and  $2.0$ . In particular, the solid curves represent Hartree-Slater results, and the chained curves hydrogenic-approximation results. In either case, the curve lying highest at smallest  $(Ka_0)^2$  corresponds to  $\epsilon/R = 0$ ; the curve lying next highest at smallest  $(Ka_0)^2$  corresponds to  $\epsilon/R = 0.5$ , and so on. In other words, the optical limit  $df(0,E)/d(E/R)$  is monotonically decreasing with  $\epsilon$ , as is always the case for the hydrogenic-approximation.

Nevertheless, Fig. 7a illustrates a sharp difference of the Hartree-Slater results from the hydrogenic-approximation results. First of all, the magnitude at  $(Ka_0)^2 \rightarrow 0$  is less than half the hydrogenic-approximation value at  $\epsilon/R = 0$ . Second, the same magnitude stays virtually constant for the range  $0.5 \leq \epsilon/R \leq 2.0$ , while the hydrogenic-approximation value decreases steadily with increasing  $\epsilon/R$ . Finally, in the same  $\epsilon$  range, the Hartree-Slater results show the gradual development of the maximum at a high  $(Ka_0)^2$  value, i.e., the emergence of the Bethe ridge.

In Fig. 7b, one begins to observe the approach to the hydrogenic behavior. Here, the solid curves represent the Hartree-Slater results for  $\epsilon/R = 3, 4, 5, 6,$  and  $8$ , in the order of decreasing height at low  $(Ka_0)^2$ ; the chained curves represent the hydrogenic-approximation results for the same  $\epsilon/R$  values also in the order of decreasing height. Throughout the  $\epsilon$  range of Fig. 7b, the Hartree-Slater results indicate the full development of the Bethe ridge. In contrast, the hydrogenic-approximation results begin to show the Bethe ridge only belatedly with increasing  $\epsilon$ .

In Fig. 7c, one sees the virtual agreement with the hydrogenic-approximation. The curves show results for  $\epsilon/R = 10, 15, 20, 25,$  and  $30$  in the order of decreasing height; this applies to both the Hartree-Slater results (shown by the solid curves) and the hydrogenic-approximation results.

Figure 8 concerns the ionization of the 2p-subshell, which has the binding energy  $B = 81$  eV. Figure 8a shows results for the same set of the lowest  $\epsilon$  values,  $\epsilon/R = 0, 0.5, 1.0, 1.5,$  and  $2.0$ . The chained curves are based on the hydrogenic-approximation, and show the monotonic decrease of the generalized oscillator strength with increasing  $\epsilon$ . By sharp contrast, the Hartree-Slater values (shown by the solid curves) are increasing with increasing  $\epsilon$ ; the lowest solid curve shows the Hartree-Slater value for  $\epsilon/R = 0$ , which is less than one-tenth the corresponding hydrogenic-approximation value. Figure 8b shows results for  $\epsilon/R = 3, 4, 5, 6,$  and  $8$ . Both the Hartree-Slater results (shown by the solid curves) and the hydrogenic-approximation results (shown by the chained curves) are decreasing with increasing  $\epsilon$ . Figure 8c shows the close approach to the hydrogenic behavior, realized for  $\epsilon/R = 10, 15, 20, 25,$  and  $30$ ; the highest curve corresponds to  $\epsilon/R = 10$ , the next highest to  $\epsilon/R = 15$ , and so on.

**Fig. 7.** The generalized oscillator strength for the ionization of the 2s-subshell of aluminum.

The horizontal axis represents  $\ln[(Ka_0)^2]$  and the vertical axis represents the density  $df(K,E)/d(E/R)$  of the generalized oscillator strength per unit range of  $E/R = (\epsilon + B)/R$ , where  $\epsilon$  is the kinetic energy of an ejected electron, and  $B$  is the binding energy of the shell, or the threshold for the ionization from that shell. In this case,  $B = 127$  eV, according to Shirley et al. (1977). Figure 7a shows values for  $\epsilon/R = 0, 0.5, 1.0, 1.5, 2.0$ . Figure 7b shows values for  $\epsilon/R = 3, 4, 5, 6, 8$ . Figure 7c shows values for  $\epsilon/R = 10, 15, 20, 25, 30$ . The three sets of  $\epsilon/R$  values are standard and common to many of the figures to follow. In all plots (including the figures to follow), the solid curves represent Hartree-Slater results, and the chained curves hydrogenic-approximation results. In Fig. 7a, the curve lying highest at the smallest  $\ln[(Ka_0)^2]$  values corresponds to  $\epsilon/R = 0$ , the curve lying next highest at the smallest  $\ln[(Ka_0)^2]$  values to  $\epsilon/R = 0.5$ , and so forth.

The peculiar behavior of the 2p-generalized oscillator strength at low  $\epsilon$  and low  $K$ , in sharp disagreement from the hydrogenic-approximation results, is attributable to the phenomenon of the delayed maximum in photoabsorption cross sections.

Detailed interpretation of the delayed maximum in the 2p ionization of aluminum was given by Manson (1972b). Briefly, this arises from the  $\epsilon$ -dependence of the d-continuum final state, which is the dominant contributor to the generalized oscillator strength. [See Fig. 3 of Manson (1972b)]. At  $\epsilon/R = 0$  and small  $\epsilon/R$ , the centrifugal potential keeps the d-continuum wave out of small distances at which the initial 2p wavefunction has appreciable magnitudes, and therefore the radial matrix element [Eq. (20)] must become small. At higher  $\epsilon/R$ , the d-continuum wave begins to reach the small distances and to attain appreciable overlap with the initial 2p state. According to Eq. (25), the total effective potential

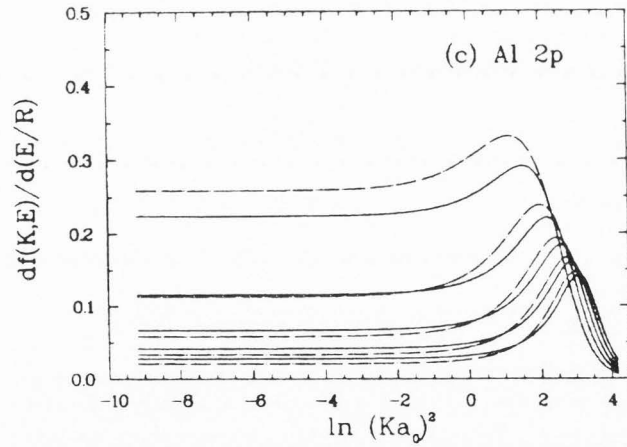
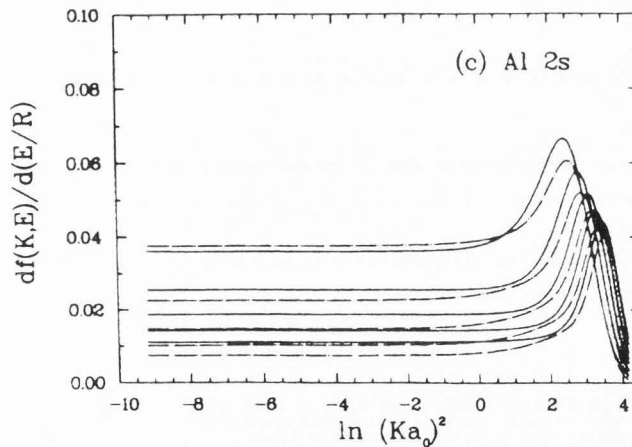
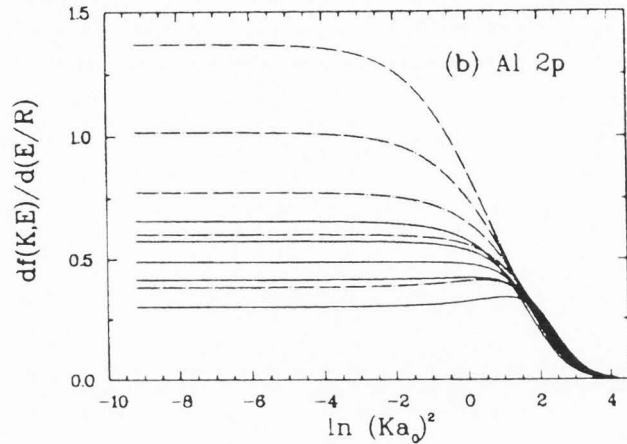
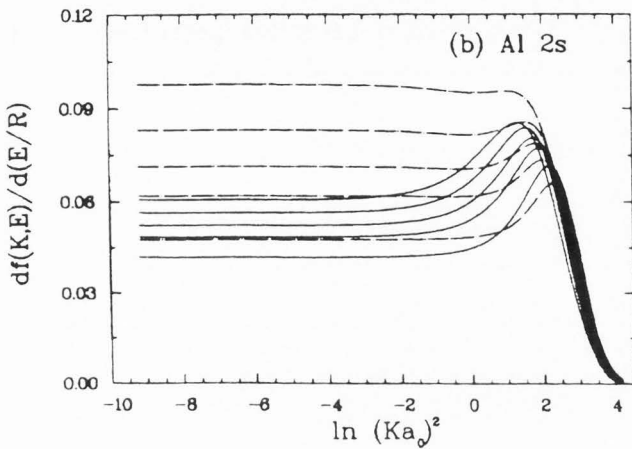
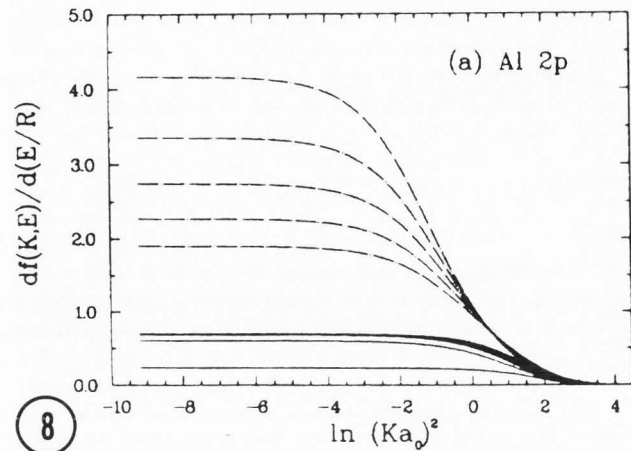
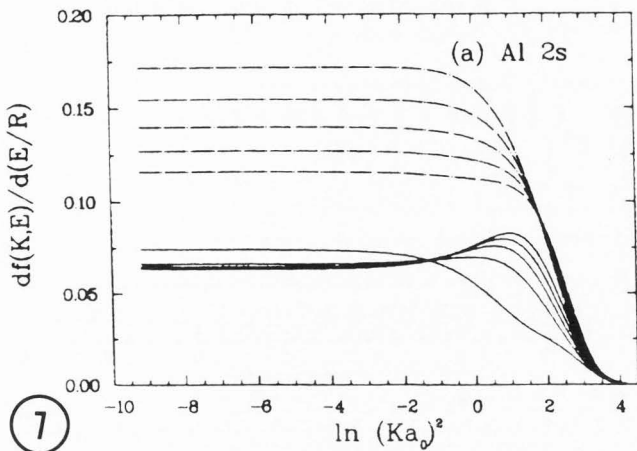
$$U(r) = V(r) + \frac{\hbar^2 \ell(\ell + 1)}{2mr^2} \quad (29)$$

with  $\ell = 2$  determines the d wave. As Fig. 9 shows,  $U(r)$  gives rise to a shallow, but wide-ranged attractive region. As a result, properties of the d-wave change markedly between  $\epsilon/R = 0$  and  $\epsilon/R = 2.0$  (see Fig. 10). For example, the phase  $\delta$  (with respect to the Coulomb wave) increases considerably with  $\epsilon$ . [See Fig. 3 of Manson (1969).] The change of  $\delta$  here is only about 0.7 radians, and the situation is different from a typical resonance, which is associated with a change of  $\delta$  by almost  $\pi$  and implies the presence of a quasi-bound state. Nevertheless, there is significant  $\epsilon$ -dependence of some d-wave properties, most notably the d-wave amplitude, which is defined as follows. According to Eq. (25), the continuum wavefunction  $P_{\ell\ell}(r)$  behaves near  $r = 0$  as

$$P_{\ell\ell}(r) = C_{\ell\ell} r^{\ell+1}, \quad (30)$$

where  $C_{\ell\ell}$  is a number, depending on  $\epsilon$  and  $\ell$ , to be determined so that the normalization relation, Eq. (26), is satis-

Cross Sections for Inelastic Scattering



fied. The determination requires knowledge of the unnormalized wavefunction over the entire  $r$  domain. Analysis shows that  $|C_{\epsilon l}|^2$  is the major factor that determines the  $\epsilon$ -dependence of the matrix element over a small  $\epsilon$  interval. It should also be noted that  $|C_{\epsilon l}|^2$  is virtually the same as the notion of the density of states, often used by solid-state theorists.

Figure 11 shows results for the ionization of the K-shell (1s shell) of aluminum. For simplicity, we include in Fig. 11a results for two values of ejected-electron energy, i.e.,  $\epsilon/R = 0$

Fig. 8. The generalized oscillator strength for the ionization of the 2p-subshell of aluminum.

The threshold energy  $B$  is 81 eV according to Shirley et al. (1977). The standard sets of  $\epsilon/R$  values are used for Fig. 8a, Fig. 8b, and Fig. 8c. Most of the captions to Fig. 7 apply here. As an exception, in Fig. 8a only, the Hartree-Slater results (shown by solid curves) are increasing with increasing  $\epsilon$ ; in other words, the lowest-lying solid curve corresponds to  $\epsilon/R = 0$ , the next lowest curve to  $\epsilon/R = 0.5$ , and so forth.

**Fig. 9.** The total effective potential for a d electron ( $\ell = 2$ ) emerging from the aluminum atom.

The potential  $U$  is defined by Eq. (29) of the text, and its value measured in  $R$  is here plotted against distance  $r$  measured in  $a_0$ . Figure 9a shows the Hartree-Slater potential over the wide range of  $r$ . Note the bump around  $r/a_0 = 3.3$ . Even though the top of the hump is below zero energy, the potential gives rise to the marked difference in the behavior of the radial functions for  $\epsilon/R = 0$  and  $\epsilon/R = 2$ , shown in Fig. 10. Figure 9b shows the Hartree-Slater potential (plotted as the solid curve) at small  $r$ . It also shows the potential used in the hydrogenic approximation (plotted as the chained curve). Note the logarithmic vertical scale. The two potentials are similar in the small region  $r/a_0 < 0.3$  (except at the close vicinity of the nucleus not shown here), but differ greatly for large  $r$ ; in particular, the hydrogenic potential stays positive throughout, and approach  $V_0/R = 6.82$  [See Eq. (27).]

$\epsilon/R = 0.5$ . The hydrogenic-approximation results (shown in the chained curves) are decreasing with  $\epsilon$ : the upper curve refers to  $\epsilon/R = 0$ , and the lower one to  $\epsilon/R = 0.5$ . The Hartree-Slater results (shown in the solid curves) are opposite in the order: the lower curve refers to  $\epsilon/R = 0$ , and the upper one to  $\epsilon/R = 0.5$ . Here again, the non-monotonic behavior in  $\epsilon$  is attributable to that of  $|C_{\ell}|^2$ .

Before concluding this Subsection, we point out the generality of many observations we made above. First of all, the non-hydrogenic behavior of the generalized oscillator is seen in all atoms we studied, whenever the kinetic energy  $\epsilon$  of an ejected electron is small or comparable to the atomic potential in the relevant spatial region. Second, the delayed maximum is common to many instances of  $p - d$  transitions, where the final d-wave is governed by the effective potential  $U$  having a well-and-hump structure. Actually, the case of d-waves for chlorine, argon, or potassium shows a much more pronounced hump, and the delayed maximum is much more prominent (see Fig. 12). Third, the near-threshold structure of the kind we saw in the K-shell ionization of aluminum is common to most atoms (Manson and Inokuti 1980, and Holland et al. 1978). To illustrate the common occurrence of the non-hydrogenic behavior, Figs. 13-15 show selected results.

We should also note that there are many other ways for showing data than the Miller-Platzman plot (which is the most fundamental). For instance, one could show the generalized oscillator strength as a function of  $\epsilon$ , either at fixed  $K$  or at fixed  $\theta$ . We may call the result a spectral plot. Figure 16 is an example. A spectral plot of the differential cross section  $d\sigma_E/d\omega$  at a fixed  $\theta$  is often called an electron energy loss spectrum. Often one sees in the literature an energy loss spectrum of a slightly different kind, i.e.,

$$\Delta\sigma_E = \int_0^{\hat{\theta}} (d\sigma_E/d\omega) d\omega, \quad (31)$$

plotted as a function of  $E$ , for a fixed aperture angle  $\hat{\theta}$ . Inokuti (1978) gave some general remarks on this quantity. Leapman et al. (1980) and Rez and Leapman (1981) have presented extensive results on this quantity of frequent reference in electron microscopy.

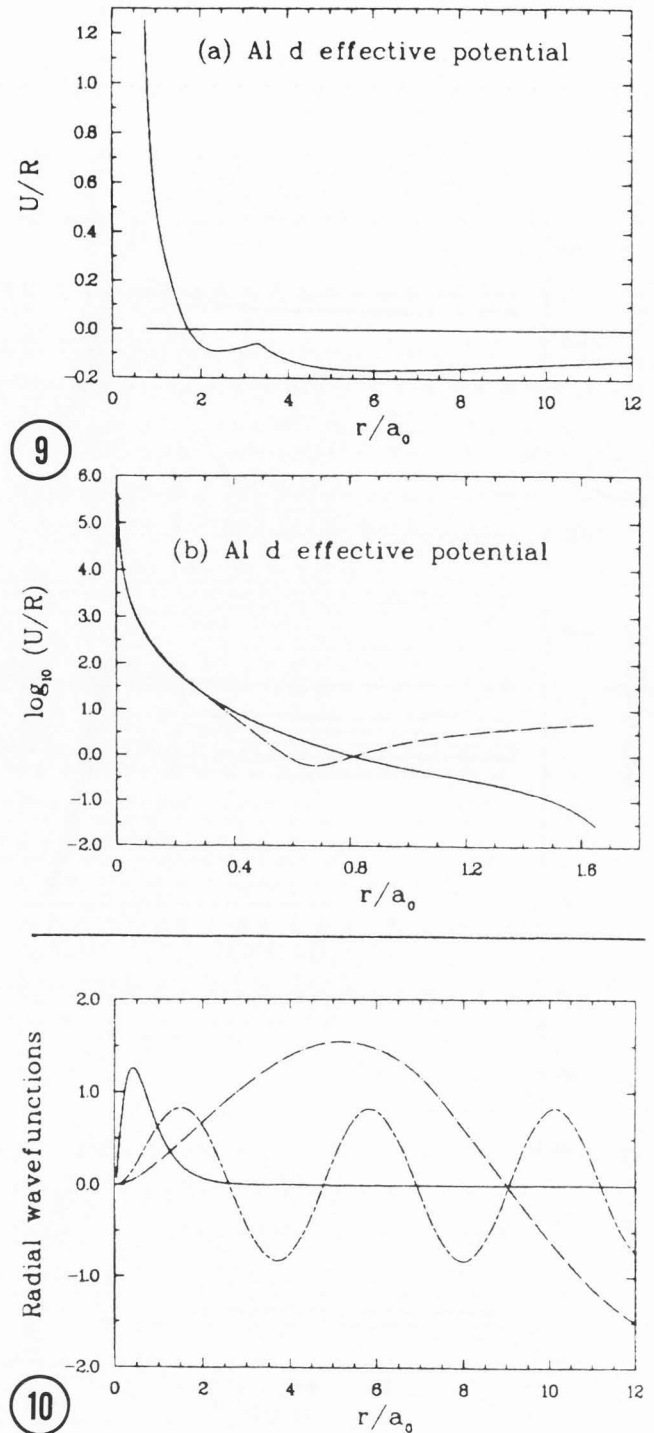


**Fig. 10.** Radial wavefunctions for the 2p state (solid curve) and the d-continuum states for aluminum.

The chained-dot curve ( $- \cdot - \cdot$ ) shows the d-continuum wave-function for  $\epsilon/R = 0$ , and the chained-dash curve ( $- - -$ ) the same for  $\epsilon/R = 2$ . The plotted values correspond to  $\pi^{-1/2} P_{\ell}^{\ell}(r)$  with  $\ell = 2$  in the notation of the text. The solid curve shows the normalized 2p bound-state. Notice that the d-continuum wavefunction for  $\epsilon/R = 2$  has a much greater overlap with the 2p state than for  $\epsilon/R = 0$ .



### Cross Sections for Inelastic Scattering

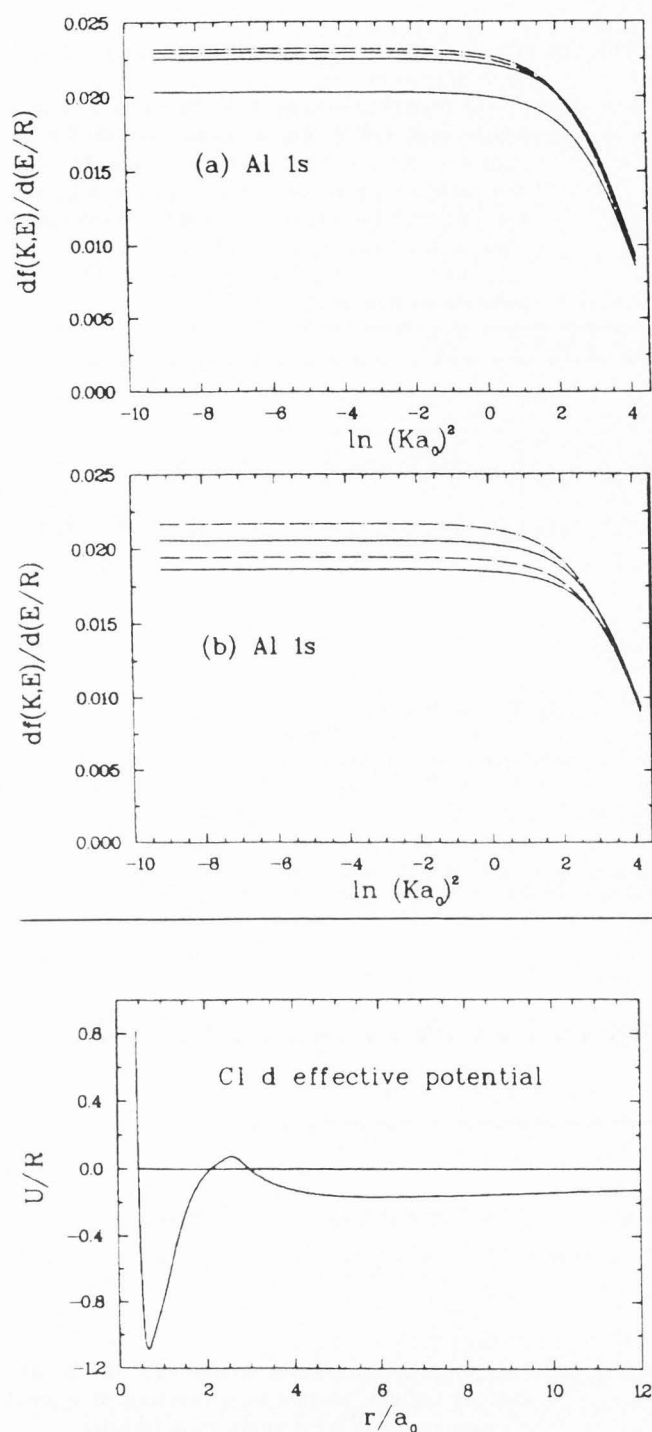


Fig. 12. The total effective potential for a d electron emerging from the chlorine atom.

The potential  $U$  is defined by Eq. (29) of the text, and its value measured in  $R$  is plotted against distance  $r$  measured in  $a_0$ . The hump around  $r/a_0 = 2.5$  stands out to positive energy, and causes a prominent delayed maximum for the  $2p \rightarrow d$  transition.

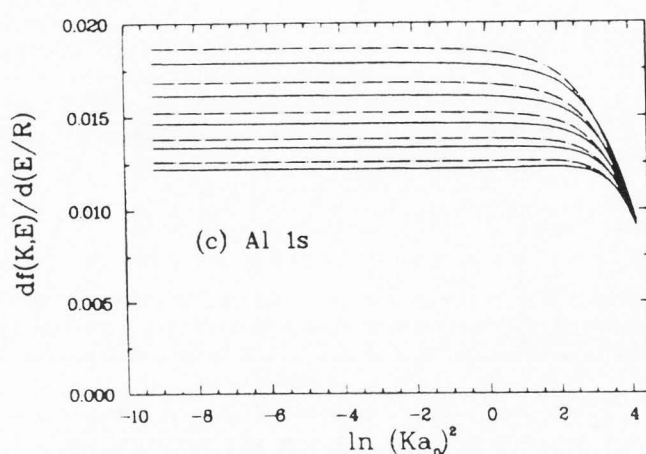


Fig. 11. The generalized oscillator strength for the ionization of the 1s-shell (or K-shell) of aluminum.

The threshold energy  $B$  is 1.57 keV, according to Shirley et al. (1977). Most of the captions to Fig. 7 apply here. An exception is Fig. 11a. In a deviation from the standard set, we show here results for  $\epsilon/R = 0$  and  $\epsilon/R = 0.5$  only. The Hartree-Slater results are shown by solid curves; the lower one corresponds to  $\epsilon/R = 0$  and the upper one to  $\epsilon = 0.5$ . The hydrogenic-approximation results are shown by chained curves; the upper one corresponds to  $\epsilon/R = 0$ , and the lower one to  $\epsilon/R = 0.5$ . Another exception is Fig. 11b, in which the upper curves (both solid and chained) correspond to  $\epsilon/R = 3$  and the lower curves to  $\epsilon/R = 8$ .

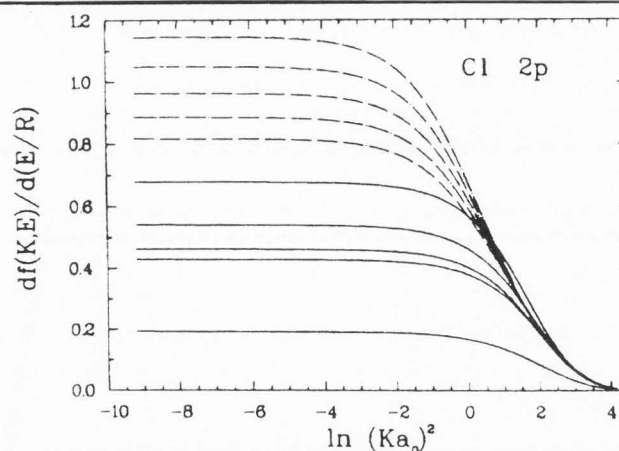


Fig. 13. The generalized oscillator strength for the 2p-subshell of chlorine.

The threshold energy  $B$  is 210 eV according to Shirley et al. (1977). The standard set of the five lowest  $\epsilon$  values ( $\epsilon/R = 0, 0.5, 1, 1.5, 2$ ) is used. The Hartree-Slater results (shown as solid curves) are much lower than the hydrogenic-approximation results (shown as the chained curves), owing to the effects of the effective potential for the d-continuum final states (shown in Fig. 12). Indeed, the Hartree-Slater results are lowest for  $\epsilon/R = 0$ , highest for 0.5, and then decreasing for larger  $\epsilon/R$ , while the hydrogenic-approximation results are decreasing steadily with increasing  $\epsilon$ .



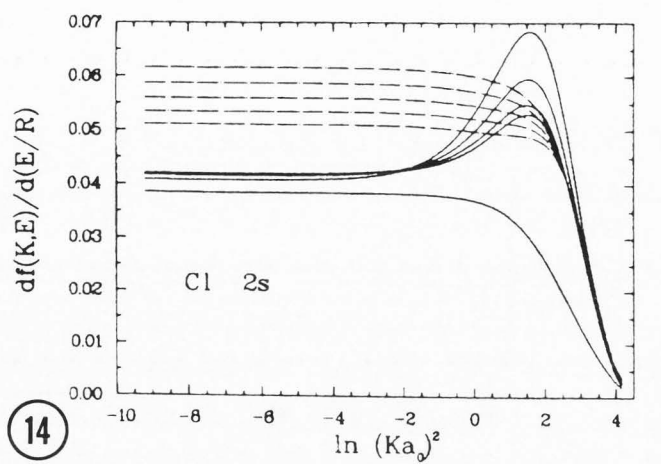


Fig. 14. The generalized oscillator strength for the 2s-subshell of chlorine.

The threshold energy  $B$  is 278 eV according to Shirley et al. (1977). The standard set of the lowest  $\epsilon$  values ( $\epsilon/R = 0, 0.5, 1, 1.5, 2$ ) is used. The Hartree-Slater results (shown as the solid curves) are increasing with increasing  $\epsilon$ , and indicate the emergence of the Bethe ridge, while the hydrogenic-approximation results (shown as the chained curves) indicate no sign of it.

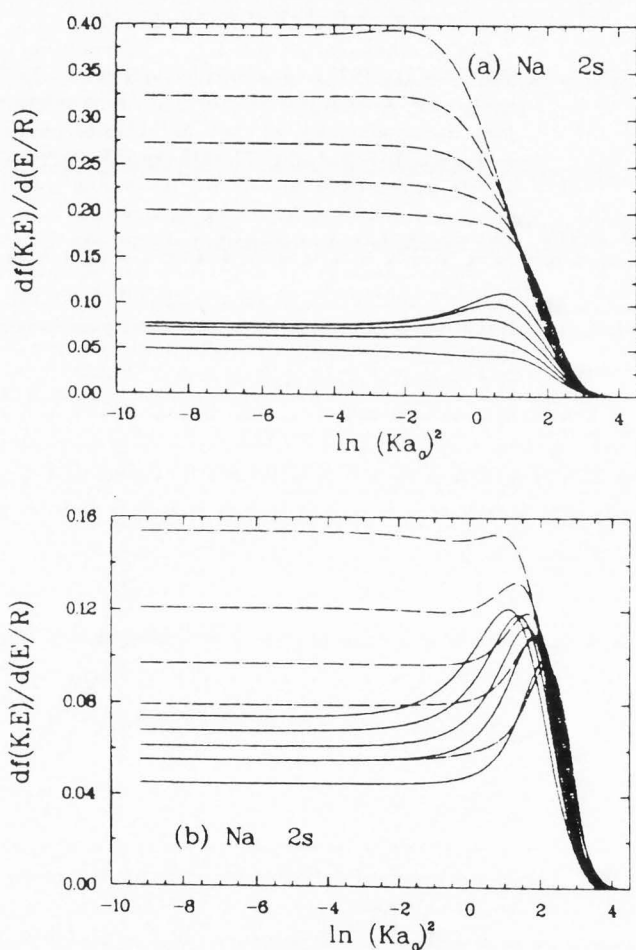


Fig. 15. The generalized oscillator strength for the 2s-subshell of sodium.

The binding energy  $B$  is 71 eV according to Shirley et al. (1977). Figure 15a shows results for the five lowest  $\epsilon/R$  values of the standard set. The Hartree-Slater results (shown as solid curves) are decreasing with increasing  $\epsilon$ , while the hydrogenic-approximation results are decreasing with increasing  $\epsilon$ . Figure 15b shows the results for the five intermediate  $\epsilon/R$  values of the standard set.

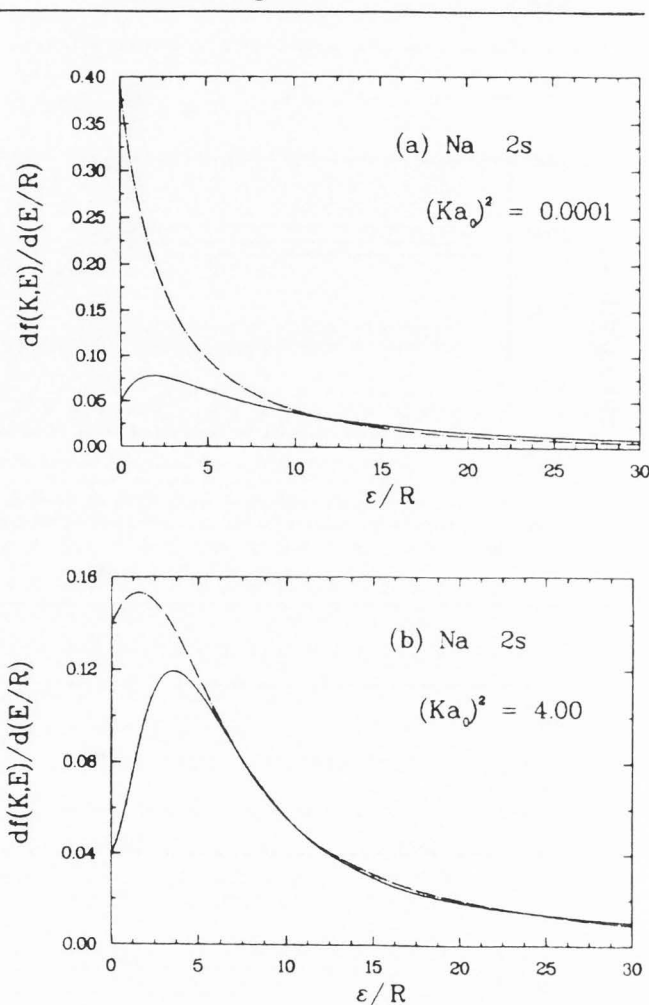


Fig. 16. The generalized oscillator strength for the 2s-subshell of sodium, plotted as a function of ejected electron energy at fixed momentum transfer.

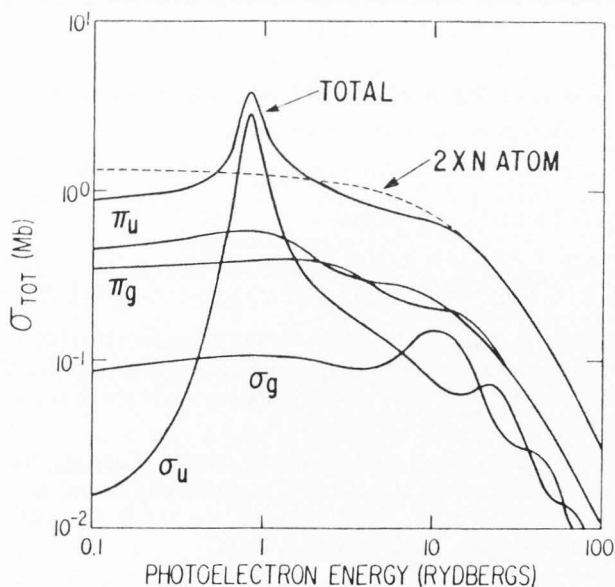
Basically the same data shown in Fig. 15 are plotted, but in a different way. The horizontal axis here represents  $\epsilon/R$ , i.e., the ejected-electron energy measured in  $R$ , at a fixed value of  $(Ka_0)^2$ . In all cases, the solid curve shows the Hartree-Slater results, and the chained curve the hydrogenic-approximation results. Figure 16a represents  $(Ka_0)^2 = 10^{-4}$ , i.e., the optical limit. Figure 16b represents  $(Ka_0)^2 = 4$ , showing an approach to the hydrogenic-approximation results and the emergence of the Bethe ridge.

## 3.3 Molecular and Solid-State Effects

In many instances we have seen much evidence for the role of atomic fields in governing the motion of an ejected electron, especially when its energy is low. For a molecule, the field of force seen by an ejected electron is in general non-spherical because of the molecular geometry. This is so even though the electronic structure of deep inner shells is affected only modestly by the molecular binding, as seen by the chemical shifts of core binding energies. [See Shirley et al. (1977) and Carlson (1975).]

Molecular effects on the optical oscillator strength, i.e.,  $df(K,E)/dE$  at  $K \rightarrow 0$ , have been recognized both experimentally and theoretically, and much of the understanding here should be pertinent to the generalized oscillator strength at finite momentum transfer. (However, there has been no extensive calculation specifically for molecules.)

Figure 17 illustrates a dramatic example of molecular effects. This figure shows the photoionization cross section (the same as  $df(K,E)/dE$  at  $K \rightarrow 0$ , apart from a universal constant) for the K-shell of molecular nitrogen, as calculated by Dehmer and Dill (1976). The calculation is based upon a single-electron picture (like the calculation on atoms we saw in Subsections 3.1 and 3.2), and upon a potential that is manifestly non-spherical. Because of the molecular geometry, one must distinguish four final-state classes designated by symbols  $\sigma_g$ ,  $\sigma_u$ ,  $\pi_g$ ,  $\pi_u$ , as opposed to the single class (the p state) for an atom. Whereas three of the classes show a smooth behavior for lower energies  $\epsilon$  of ejected electrons, the  $\sigma_u$  symmetry gives rise to a sharp peak at about  $\epsilon/R = 1.2$ , and causes a marked difference from the atomic case. According to Dehmer and Dill (1976), the origin of the peak is a shape resonance, i.e., the appearance of a quasi-bound state in the molecular potential field. Roughly speaking, an electron in the  $\sigma_u$  state at that energy is temporarily trapped by the field before escaping out eventually. *The shape resonance is a general occurrence for many molecules.* Indeed, a review article by Dehmer and Dill (1979) shows many other examples.



In solid-state contexts, effects analogous to the shape resonance are often called XANES (x-ray absorption near-edge structure), and have been the subject of many recent studies. Examples of theoretical studies include Durham et al. (1981) and Durham et al. (1982).

One sees another feature that distinguishes the molecule from the atom. That is to say, there are undulations at higher energies  $\epsilon \geq 10 R$  in all the four symmetry classes. (However, the undulations in the  $\pi_u$  and  $\pi_g$  symmetry classes are too small to be seen in Fig. 17.) These undulations were recognized much earlier, and are known as EXAFS (extended x-ray absorption fine structures). [See Teo and Joy (1981) for example.] Briefly, the undulations result from constructive and destructive interference of ejected-electron waves with those scattered from different atoms. The variation with energy is roughly represented by  $\sin(kD)$ , where  $k = (\epsilon/R)^{1/2}/a_0$  is the wave number of the ejected electron and  $D$  is the internuclear distance. Because of the origin, it is easy to see that the EXAFS is in principle universal to all molecules and solids, even though the size of the undulations is often small and the pattern is more complicated for cases involving many and different atoms. Indeed the notion of the EXAFS is so well-known and prevailing in solid-state physics that Holland et al. (1978) adapted an EXAFS theory to interpret the near-threshold structure of atomic K-shell spectra.

The shape resonance and the EXAFS are two well recognized molecular effects. In reality, there are further effects contributing to the near-edge structure of inner-shell spectra of molecules and solids. Indeed, the electron energy loss spectrum obtained experimentally by Wight et al. (1972/73), shown as Fig. 18, indicates peaks additional to the shape-resonance peak. [Note that the energy loss spectrum in the forward scattering is roughly  $E^{-3} df(0,E)/dE$ , plotted as a function of  $E$  and is thus distorted from the optical oscillator-strength spectrum. See Sec. 3.1 of Inokuti (1971).] Some of the additional peaks are attributed to effects beyond the single-electron picture, e.g., simultaneous excitation of another electron along with the inner-shell ionization.

In conclusion, we may reiterate that there has been no calculation of the generalized oscillator strength of inner shells specifically including molecular or solid-state effects. Yet, the developments described above suggest that there is already enough groundwork for such a calculation, in both concepts and techniques and that the time may be ripe for a major undertaking.

Fig. 17. Photoionization cross section of the K-shell of molecular nitrogen.

The figure is reproduced here with permission from Dehmer and Dill (1976). The horizontal axis represents the kinetic energy of an ejected electron measured in Rydbergs, and corresponds to  $\epsilon/R$  in the text of the present paper. The vertical axis represents the photoionization cross section  $\sigma_{TOT}$  measured in Mb =  $10^{-18}$  cm<sup>2</sup>, which is related to the density of the optical oscillator strength by  $\sigma_{TOT} = 4\pi^2(e^2/hc) a_0^2 df(0,E)/d(E/R) = 8.067 \times df(0,E)/d(E/R) \times 10^{-18}$  cm<sup>2</sup>. Each of the solid curves shows contributions from the indicated class of final-state symmetry. The dashed curve shows twice the photoionization cross section of the K-shell of atomic nitrogen.

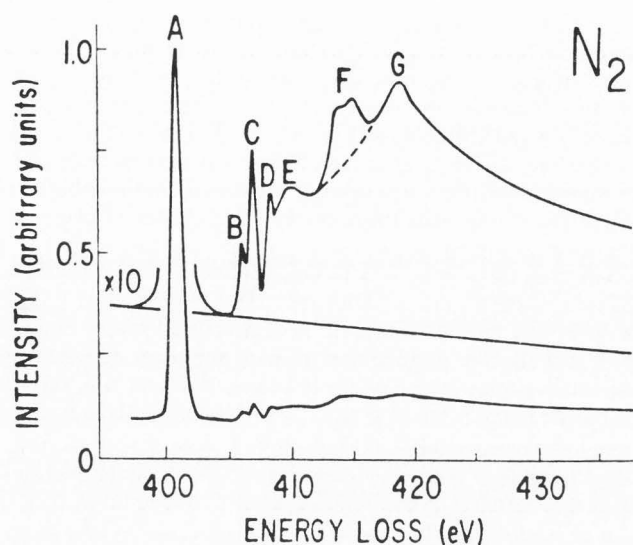


**Fig. 18.** Electron energy-loss spectrum of molecular nitrogen in the neighborhood of the K-shell threshold (409.9 eV).

The figure is reproduced here with permission from Wight et al. (1972/73). The vertical axis represents the intensity of electrons scattered into the forward direction, the incident energy being 2.5 keV. The strongest peak (labeled as A) corresponds to the shape resonance discussed by Dehmer and Dill (1976). The other peaks (labeled as B, C, D, E, F, and G) are attributable to other phenomena that are outside the scope of the present article.

#### ACKNOWLEDGEMENTS

We thank C.E. Brion, J.L. Dehmer, J. Geiger, and H.F. Wellenstein for their generous permission and assistance for reproducing here figures or data from their publications.

#### REFERENCES

- Barlas AD, Ruekner W, Wellenstein HF. (1977). High energy electron impact spectroscopy measurement on the Compton effect. *Phil. Mag.* **36**, 201-207.
- Bethe H. (1930). Zur Theorie des Durchgangs schneller Korpuskularstrahlen durch Materie. *Ann. Phys. (Leipzig)* **5**, 325-400.
- Bethe H. (1932). Bremsformel für Elektronen relativistischer Geschwindigkeiten. *Phys.* **76**, 293-299.
- Bethe H. (1933). Quantenmechanik der Ein- und Zwei-Elektronenprobleme. Chapter 3 in *Handbuch der Physik*, (H. Geiger and K. Scheel, eds.), Verlag von Julius Springer, Berlin, Vol. 24/1, 273-560.
- Bohr N. (1948). The penetration of atomic particles through matter. *K. Dan. Videns. Selsk., Mat. Fys. Medd.* **18**, No. 8, 1-144.
- Bonham RA and Wellenstein HF. (1973). Measurements of quantities related to the charge and momentum densities of atoms and molecules by use of keV electron scattering. *Int. J. Quantum Chem. Symp. No. 7*, 377-394.
- Carlson TA. (1975). *Photoelectron and Auger Spectroscopy*, Plenum Press, New York.
- Dehmer JL and Dill D. (1976). Molecular effects on the inner-shell photoabsorption. K-shell spectrum of  $N_2$ . *J. Chem. Phys.* **65**, 5327-5334.
- Dehmer JL and Dill D. (1979). The continuum multiple-scattering approach to electron-molecule scattering and molecular photoionization, in: *Electron-Molecule and Photon-Molecule Collisions*, T. Rescigno, V. McKoy, and B. Schneider (eds.), Plenum Press, New York, 225-265.
- Durham PJ, Pendry JB, and Hodges CH. (1981). XANES: Determination of bond angles and multi-atom correlations in order and disordered systems. *Solid State Commun.* **38**, 159-162.
- Durham PJ, Pendry JB, and Hodges CH. (1982). Calculation of x-ray absorption near-edge structure. *Comput. Phys. Comm.*, **25**, 193-205.
- Fano U. (1956). Atomic theory of electro-magnetic interactions in dense materials. *Phys. Rev.* **103**, 1202-1218.
- Fano U and Cooper JW. (1968). Spectral distribution of atomic oscillator strength. *Rev. Mod. Phys.* **40**, 441-507.
- Fano U, Theodosiou CE, and Dehmer JL. (1976). Electron-optical properties of atomic fields. *Rev. Mod. Phys.* **48**, 49-68.
- Fermi E. (1940). The ionization loss of energy in gases and condensed materials. *Phys. Rev.* **57**, 485-493.
- Ferrell RA. (1957). Characteristic energy loss of electrons passing through metal foils: II. Dispersion relation and short wavelength cutoff for plasma oscillations. *Phys. Rev.* **107**, 450-462.
- Geiger J. (1964). Streuung von 25 keV-Elektronen an Gasen. II. Streuung an Neon, Argon, Krypton und Xenon. *Z. Phys.* **177**, 138-145.
- Holland BW, Pendry JB, Pettifer RF, and Bordas J. (1978). Atomic origin of structure in EXAFS experiments. *J. Phys. C.* **11**, 633-642.
- Inokuti M. (1971). Inelastic collisions of fast charged particles with atoms and molecules—The Bethe theory revisited. *Rev. Mod. Phys.* **43**, 297-347.
- Inokuti M. (1978). Electron-scattering cross sections pertinent to electron microscopy. *Ultramicroscopy* **3**, 423-427.
- Inokuti M, Dehmer JL, Baer T, and Hanson JD. (1981). Oscillator-strength moments, stopping powers, and total inelastic-scattering cross sections of all atoms through strontium. *Phys. Rev. A.* **23**, 95-109.
- Inokuti M, Itikawa Y, and Turner JE. (1978). Addenda: Inelastic collisions of fast charged particles with atoms and molecules—The Bethe theory revisited [*Rev. Mod. Phys.* **43**, 297 (1971)]. *Rev. Mod. Phys.* **50**, 23-35.

## Cross Sections for Inelastic Scattering

- Inokuti M, Kim Y.-K., and Platzman RL. (1967). Total cross sections for inelastic scattering of charged particles by atoms and molecules. I. A sum rule for the Bethe cross sections and its application to the helium atom. *Phys. Rev.* **164**, 55-61.
- Inokuti M and Turner JE. (1978). Mean excitation energies for stopping power as derived from oscillator-strength distributions, in: *Proceedings of the Sixth Symposium on Microdosimetry*, Brussels, 1978, J. Booz and H.G. Ebert (eds.), Harwood Academic Publishers, London, 675-687.
- Khandelwal GS and Merzbacher E. (1966). Stopping power of M electrons. *Phys. Rev.* **144**, 349-352.
- Lahman-Bennani A, Duguet A, and Wellenstein HF. (1979). Bethe surface and Compton profile for CO<sub>2</sub> obtained by use of 35-keV incident electrons. *Chem. Phys. Lett.* **60**, 405-410.
- Lahman-Bennani A, Duguet A, Wellenstein HF, and Ronault M. (1980). Bethe surface and Compton profile of NH<sub>3</sub> obtained by 35-keV electron impact. *J. Chem. Phys.* **72**, 6398-6408.
- Landau LD and Lifshitz EM. (1960). *Electrodynamics of Continuous Media*, translated by J.B. Sykes and J.S. Bell, Pergamon, London. See Chapters IX and XII in particular.
- Lassetre EN, Skerbele A, and Dillon MA. (1969). Generalized oscillator strength for 1<sup>1</sup>S → 2<sup>1</sup>P transition of helium. Theory of limiting oscillator strength. *J. Chem. Phys.* **50**, 1829-1839.
- Leapman RD, Rez P, and Mayers DF. (1980). K-, L-, and M-shell generalized oscillator and strengths and ionization cross sections for fast electron collisions. *J. Chem. Phys.* **72**, 1232-1243.
- Manson ST. (1969). Dependence of the phase shift on energy and atomic number for electron scattering by atomic fields. *Phys. Rev.* **182**, 97-103.
- Manson ST. (1972a). Theoretical study of generalized oscillator strengths in atoms: Comparison with experiment and other calculations. *Phys. Rev. A.* **5**, 668-677.
- Manson ST. (1972b). Inelastic collisions of fast charged particles with atoms: Ionization of the aluminum L-shell. *Phys. Rev. A.* **6**, 1013-1024.
- Manson ST. (1976). Atomic photoelectron spectroscopy, Part I, in: *Advances in Electronics and Electron Physics*, L. Marton (ed.), Academic Press, New York, Vol. 41, 73-111.
- Manson ST. (1977). Atomic photoelectron spectroscopy, Part II, in: *Advances in Electronics and Electron Physics*, L. Marton (ed.), Academic Press, New York, Vol. 44, 1-32.
- Manson ST. (1978). The calculation of photoionization cross sections; An atomic view, in: *Topics in Applied Physics*, Vol. 26, Photoemission in Solids, I. General Principles, M. Cardona and L. Ley (eds.), Springer-Verlag, Berlin, 135-163.
- Manson ST and Dill D. (1978). The photoionization of atoms: Cross sections and photoelectron angular distributions, in: *Electron Spectroscopy, Theory, Techniques, and Applications*, C.R. Brundle and A.D. Baker (eds.), Academic Press, New York, Vol. 2, 157-195.
- Manson ST and Inokuti M. (1980). Near-threshold structure in the atomic K-shell spectra for ionization by photons or fast charged particles. *J. Phys. B.* **13**, L323-L326.
- Matsuzawa M, Mitsuoka, and Inokuti M. (1979). Integrals of the squared atomic form factor over the momentum transfer. *J. Phys. B.* **12**, 3033-3046.
- McCarthy IE and Weigold E. (1976). (e,2e) Spectroscopy. *Phys. Rep.* **27**, 275-371.
- McGuire EJ. (1977). Scaled electron ionization cross sections in the Born approximation. *Phys. Rev. A.* **16**, 73-79.
- McGuire EJ. (1979). Scaled electron ionization cross sections in the Born approximations for atoms with  $55 \leq Z \leq 102$ . *Phys. Rev. A.* **20**, 445-456.
- Miller WF and Platzman RL. (1957). On the theory of the inelastic scattering of electrons by helium atoms. *Proc. Phys. Soc. (London)*, **70**, 299-303.
- Nozières P and Pines D. (1959). Electron interaction in solids. Characteristic energy loss spectrum. *Phys. Rev.* **113**, 1254-1267.
- Powell JC. (1983). Inelastic scattering of electrons in solids, in: *Electron Beam Interactions, SEM, Inc., AMF O'Hare, IL*, 19-31.
- Raether H. (1980). *Excitation of Plasmons and Interband Transitions by Electrons*, Springer-Verlag, Berlin.
- Rau ARP and Fano U. (1968). Atomic potential wells and the periodic table. *Phys. Rev.* **167**, 7-10.
- Rez P. and Leapman RD. (1981). Core loss shape and cross section calculations, in: *Analytical Electron Microscopy—1981*, R.H. Geiss (ed.), San Francisco Press, San Francisco, 181-186.
- Shiles E, Sasaki T, Inokuti M, and Smith DY. (1980). Self-consistency and sum-rule tests in the Kramers-Kronig analysis of optical data: Applications to aluminum. *Phys. Rev. B.* **22**, 1612-1628.
- Shirley DA, Martin RL, Kowalczyk SP, McFeely FR, and Ley L. (1977). Core-electron binding energies of the first thirty elements. *Phys. Rev. B.* **15**, 544-552.
- Starace AF. (1982). Theory of Atomic Photoionization, in: *Handbuch der Physik*, S. Flügge (ed.), Springer, Berlin, Vol. 31, 1-121.
- Teo BK and Joy C. (eds.) (1981). *EXAFS Spectroscopy*, Plenum Press, New York.
- Walske MC (1952). The stopping power of K-electrons. *Phys. Rev.* **88**, 1283-1289.
- Walske MC. (1956). Stopping power of L-electrons. *Phys. Rev.* **101**, 940-944.
- Wight GR, Brion CE, and van der Wiel MJ. (1972/73). K-shell energy loss spectra of 2.5 keV electrons in N<sub>2</sub> and CO. *J. Electron Spectrosc. Rel. Phenom.* **1**, 457-469.
- Wong TC, Lee JS, Wellenstein HF and Bonham RA. (1975). Experimental definition of valence shell and cumulative-shell Compton profiles from 25-keV electron-impact studies on N<sub>2</sub>, Ne, and Ar. *Phys. Rev. A.* **12**, 1846-1858.